

CVD Molybdenum Disulfide/Graphene Heterostructures: Synthesis and Electrochemical Applications

BY

Amirhossein Behranginia

B.S., Science and Research Branch of Azad University, Tehran, Iran, 2010

THESIS

Submitted as partial fulfillment of the requirements
for the degree of Master of Science in Mechanical Engineering
to the Graduate College of the
University of Illinois at Chicago, 2016

Chicago, Illinois

Defense Committee:

Amin Salehi-Khojin, Chair and Advisor
Jeremiah Abiade
Robert Klie, Physics

*To my parents,
and to my friends.*

ACKNOWLEDGMENTS

This thesis paper could not be written without the help and support of Dr. Amin Salehi-Khojin, who served as my supervisor, gave me support and assistance, and provided me with motivation and encouragement throughout the entire period of my research thus far at the Nanomaterials and Energy Systems Laboratory. My deepest gratitude goes also to my family and friends for their moral support. I also wish to thank Mohammad, Poya, Bijandra, Reza, Tara and all of my collaborators who helped me to complete this thesis.

AUTHORS CONTRIBUTIONS

The results and discussions in this thesis are copied from my published paper with written permission from the journal (see appendix). Below, the contributions of all the co-authors are listed:

Authors' contributions in chapter 2, 3 and 4 (copied from reference 1): A.S.K., A.B., M. A. conceived the idea. A.B. synthesized the CVD MoS₂ 3D structure. M.A. and B.K. performed the electrochemical experiments. P.Y., B.K. and K.K. synthesized the CVD graphene. P.Y., B.K., T.F. and J.C.W helped in CVD MoS₂ synthesis. A.B., M.A., B.K., and P.Y carried out the characterizations. P. P., and R. K. carried out STEM and EDX. A.S.K. and J.A. jointly supervised the M.A. efforts. All of the authors contributed to the manuscript before submission. A.S.K. work was supported by University of Illinois at Chicago through the Start-up budget and Chancellor Proof of Concept award.

TABLE OF CONTENTS

<u>CHAPTER</u>	<u>PAGE</u>
CHAPTER 1: Introduction	1
1.1. MoS ₂ /Gr heterostructure for hydrogen evolution reaction	1
1.2. Literature review of graphene	2
1.2.1. Introduction	2
1.2.2. Production methods	3
1.2.3. Properties and applications.....	5
1.3. Literature review of MoS ₂	8
1.3.1. Introduction	8
1.3.2. Production methods	9
1.3.3. Properties and applications.....	12
1.4. Research Objective	15
CHAPTER 2: Synthesize and Characterization of CVD MoS₂/Gr Heterostructure .	16
2.1. Introduction.....	16
2.2. Material Synthesis and characterizations	17
2.2.1. CVD graphene Synthesis procedure and characterizations.....	17
2.2.2. CVD 3D Structured MoS ₂ Synthesis procedure and characterizations	19
2.3. Conclusion	29
Chapter3: Electrochemical experiments and DFT calculations	30

3.1. Experimental details and results	30
3.2. Density functional theory details and results	37
3.3. Conclusion	43
Chapter 4: Conclusion and future work	44
Cited literature	46
APPENDIXES	66

LIST OF TABLES

Table 1: Extracted exchange current density for different tested catalysts.....	31
--	-----------

LIST OF FIGURES

Figure 1. SEM characterization of CVD graphene.....	18
Figure 2. Raman characterization of CVD graphene..	19
Figure 3. CVD MoS ₂ temperature profile.	20
Figure 4. SEM and STEM characterization of the 3D structured MoS ₂	21
Figure 5. XPS and Raman characterization of the 3D structured MoS ₂	22
Figure 6. EDX characterization of 3D structured MoS ₂	23
Figure 7. SEM characterization of 3D structured MoS ₂	24
Figure 8. MoS ₂ CVD setup, Optical and SEM characterizations of the different structures of MoS ₂	25
Figure 9. Raman characterization of MoS ₂ from single-layer to 3D structure.....	26
Figure 10. Optical and SEM characterization from 3D structured MoS ₂	27
Figure 11. SEM characterization of 3D structured MoS ₂ grown on graphene flakes and bare substrate..	28
Figure 12. Raman characterization of 3D structured MoS ₂ /Gr heterostructure..	29
Figure 13. CV, TOF, Binding energy and Nyquist measurements.....	34
Figure 14. EIS measurements.	35
Figure 15. Electrochemical measurements.	36
Figure 16. TOF at different current density and stability Tests.....	37
Figure 17. Atomic configuration.	38
Figure 18. PDOS graph.	39
Figure 19. Hydrogen binding energy graph.....	40
Figure 20. Reaction free energies pathway graph.	41
Figure 21. Activity relationship for HER.	42

LIST OF ABBREVIATIONS AND NOMENCLATURE

CH ₄	methane
(NH ₄) ₂ MoS ₄	ammonium thiomolybdate
2D	two-dimensional
3D	three dimensional
AFM	atomic force microscopy
APCVD	atmospheric-pressure chemical vapor depositio
Ar	Argon
C _{dl}	layer capacitor
CV	Cyclic voltammetry
CVD	chemical vapor deposition
DFT	density functional theory
DMF	dimethylformamide
DOS	density of states
EBL	electron beam lithography
EDX	energy dispersive X-ray spectroscopy
EIS	electrochemical impedance spectroscopy
FET	field-effect transistor
FFT	fast Fourier transforms
Gr	Graphene
H ₂	Hydrogen
H _{ad}	adsorbed hydrogen
HCL	Hydrochloric acid
HER	hydrogen evolution reaction
HRTEM	high resolution transmission electron microscop
IPA	isopropyl alcohol
ML	monolayer
Mo	Molybdenum
MoS ₂	Molybdenum disulfide
MOSFET	metal-oxide-semiconductor field-effect transist
N ₂	nitrogen
PDOS	Partial density of states
PMMA	Poly(methyl methacrylate)

R_{ct}	charge transfer resistances
RDS	rate determining step
RF	roughness factor
RHE	reference hydrogen electrode
S	Sulfur
Sccm	standard cubic centimeter
SDD	silicon drift detector
SEM	scanning electron microscopy
SK	Stranski-Krastanov
STEM	scanning transmission electron microscopy
TEM	transmission electron microscopy
TMD	transition metal dichalcogenides
TOF	turn over frequency
vdw	van der Waals

SUMMARY

There is a rising demand to substitute fossil fuels with environmental-friendly energy resources. Providing hydrogen resource through a water splitting process can be one way to satisfy this critical need. The high cost of the conventional water splitting catalysts such as platinum makes this process inapplicable for industry utilization. Hence, there is a need to find low cost catalysts to make this process applicable for future applications. In this respect, earth abundant and inexpensive MoS_2 nanostructures with sulfur (s) terminated edge atoms have previously been tested for HER activity. However, results indicate less efficient HERs on these structures which is mainly attributed to: (i) a low electrochemical activity of sulfur edge atoms, and (ii) a high charge transfer resistance between semiconductor MoS_2 and electrode due to the Schottky barrier formation at their interface.

In this work, a large-area crystalline 3D structured MoS_2 /Graphene (Gr) heterostructure is directly grown on the glass carbon electrodes using a large-scale atmospheric pressure chemical vapor deposition (APCVD) technique to considerably increase the active edge atoms of the MoS_2 and improve the charge transfer toward active edge sites. The grown 3D structured MoS_2 with Mo terminated edges has shown remarkable electrochemical activity due to the high density of d orbital electrons of the edge atoms (Mo). Our recent work published in chemistry of materials[1], which is widely reviewed in the second and third chapters of this dissertation, has fully investigated the growth mechanisms of this structure and the applicability of its heterostructure with graphene for HER activity. The control

experiments and characterizations have revealed that the 3D structured MoS₂ follows the Stranski-Krastanov growth mode in which the transition from 2D to 3D happens after a critical thickness. The turn over frequency (TOF) measurements have shown a very high value for the 3D structured MoS₂ demonstrating high chemical activity of this structure. Also, the electrochemical impedance spectroscopy (EIS) measurements have shown that the charge transfer resistance is much lower in 3D structured MoS₂ grown on graphene film than those grown on glassy carbon and transferred to glassy carbon. These results confirm that the growth of this structure on top of the graphene film considerably improved the contact resistance between MoS₂ and electrode.

CHAPTER 1: Introduction

1.1. MoS₂/Gr heterostructure for hydrogen evolution reaction

Rising the global energy demand in future will significantly increase the amount of the produced carbon dioxide from consuming of the fossil fuels which can drastically change the earth's climate. This serious challenge makes scientists think about replacing the fossil fuels with other environmental-friendly energy resources. Hydrogen is one option to be used as an energy resource for current devices, and one way to produce hydrogen is electrochemical water splitting[2], [3]. This process needs using a catalyst which is very active and stable for HER. Noble metals and some of the two dimensional (2D) materials are very promising for this reaction. Due to earth abundancy and low cost of 2D materials, utilizing them as a catalyst is preferable than platinum, which is a very active catalyst but expensive. Molybdenum disulfide is one of the 2D materials that attracts much attention for this application[4]–[7] because of its high activity and stability. However, the use of MoS₂ as a catalyst was not very efficient for HER reaction due to the semiconductor nature of this material. The Schottky barrier formation at the interface of the electrode and MoS₂ would increase the interface resistance and considerably decrease charge transfer through the interface. Hence, to increase the electron transfer from the electrode to the active edge sites of the MoS₂, there is a need for an interlayer materials that are not only conductive but also compatible with MoS₂ and electrochemical applications. Graphene, as a conductive and chemically inert

material[8] which also can be used as a supportive layer for the MoS₂, is a good candidate to overcome the mentioned issue. Hence, different synthesized MoS₂/Graphene (MoS₂/Gr) heterostructures can be very promising structures for dramatically improving the HER efficiency.

1.2. Literature review of graphene

1.2.1. Introduction

Graphene, a semimetal sp²-hybridized carbon sheet, is the forerunner of the 2D materials which has been the subject of much research during the past decade. Thermodynamic calculations make scientists believe that 2D materials are unstable at room temperature[9]; however, the discovery of the single layer graphene in 2004 by mechanical exfoliation of the graphite film changed the material science world [10]. Van der Waals force between the graphene layers and its substrate creates a golden opportunity for the scientist to be able to discover the intrinsic properties of graphene. Long-range π -conjugation in graphene makes it a miracle material with astonishing mechanical, electrical and thermal properties [9], [11]. Experimental measurements show the electron mobility of 2.5×10^5 cm²/V.S[12], the thermal conductivity of ~5000 Wm/K[13], the Young's module of 1Tpa[14] and many other superior properties for graphene, which makes it promising to be used for future generation devices.

Although the work on graphene was first started with the aim of studying its fundamental properties, this trend expeditiously has changed to discovering its potential

in the industry applications [15]–[17]. Hence, other methods of production have to be utilized in order to make the mass production of the graphene possible for market applications. Liquid phase exfoliation, thermal exfoliation and chemical vapor deposition[11] are the methods which have been used to synthesize large area graphene films. These methods of production are discussed briefly in the following section.

1.2.2. Production methods

1.2.2.1. Chemical exfoliation

This method is used for the production of graphene sheets. The first step is to oxidize the graphite by using strong acids and oxidants[18]. Then, the graphene oxide sheets are exfoliated by sonicating the graphite oxide sheets. The exfoliated graphene oxide sheets, which are insulators, can be suspended homogeneously in aqueous, organic or polar solvents. Finally, these insulator graphene oxide sheets can be modified to the electrically conductive reduced graphene oxide sheets by using chemical methods, thermal methods and ultraviolet assisted methods[19], [20]. It is worth mentioning that these methods cannot produce a pristine graphene due to the presence of the considerable amount of the oxygen in the reduced graphene oxide sheets[21]. There are also other exfoliation methods in which graphite intercalation compounds or expandable graphite will be used instead of the graphite oxide sheets. These methods produce high-quality graphene sheets although the yields of single layer graphene sheets is not high[21].

1.2.2.2. Chemical vapor deposition

Growth of the graphene on the SiC substrate[22]–[25] is another method of the graphene production which is easily applicable for high-power electronic applications. In this method, sublimation of the silicon atoms at very high temperatures (above 1000 °C) results in the growth of the polycrystalline graphene layers on the substrate[11], [22]. The size of the graphene films produced by this method is in the range of the hundreds of micrometers, and the high substrate cost limits the use of this method for the growth of the graphene film[11].

The growth of the graphene on the Cu foils [26] via Chemical Vapor Deposition (CVD) is a method which has been widely used to produce high quality polycrystalline graphene films on a large scale. Methane (CH_4), hydrogen (H_2) and argon are the gases which are used for the growth of the graphene by this method. Methane gas provides carbon atoms, and hydrogen gas will activate the bonding between the Cu surface and carbon atoms. Hydrogen gas also could etch the graphene layers and have a direct effect on the shape and size of the graphene grains[27] and argon gas is used as a carrier gas. In this growth method, first single crystalline graphene islands are randomly nucleated on the Cu substrate and continue to grow larger. Next, these single crystalline islands merge together and make a grain boundary and form polycrystalline graphene film. The quality of the grown polycrystalline film depends on the quality of the single crystalline grains and how well they are stitched together[16]. The quality and shape of the single crystalline grains can be affected by the growth parameters, such as temperature[28] or

pressure[16], [26] of the growth. Basically, CVD graphene can be grown by Low pressure and atmospheric pressure methods. The former results in dendritic grain shape [26] with irregular edges[16], [26], [29], [30] and the later results in a hexagonal grain shape with edges that are mostly aligned along the zigzag direction of the graphene lattice[31], [32].

1.2.3. Properties and applications

1.2.3.1. Mechanical properties and applications

The mechanical properties of a crystalline material depends on the characteristics of its lattice crystallinity. Lee et al. measured the mechanical properties of the suspended pristine graphene, which is a crystalline material with a covalently bonded carbon atoms, with Atomic force microscopy (AFM) method[14]. In this study, they reported a non-linear elastic behavior for pristine graphene with the young modulus of 1 TPa[14]. Furthermore, graphene exhibits a brittle fracture at the strength of 130 GPa [14], which proves this material has the highest strength compared to the other ones [14], [33]. As it was mentioned previously, to be able to use graphene for industrial applications, it needs to be synthesized by a method which can be utilized for mass production. Synthesizing graphene via CVD method is one of the most promising methods for large scale production. In this method, the synthesized graphene film consists of many single crystalline islands which merges together and forms many grain boundaries. Structural defects can play a key role on changing the mechanical properties of a crystalline material[34]–[36], and since the grain boundaries are considered line defects, it is also

important to know how they will effect graphene mechanical properties. While some studies have shown that the grain boundaries weaken the mechanical properties of the graphene[37], [38], Lee et al. shows that the young modulus of the polycrystalline graphene is the same as the pristine graphene, and there is just a slight change in the stiffness of the polycrystalline graphene compared to the pristine one[39]. The change in the mechanical properties of the polycrystalline graphene in previous studies can be attributed to the post-processing steps after graphene growth or the size of the single graphene grains, which form the polycrystalline film[39]. It is worth noting that the strength of the polycrystalline graphene film can significantly be reduced if the size of the single crystalline domains were small. Owing to these astonishing mechanical properties, mixing of the composite materials and polymer-based nanocomposites with graphene can considerably enhance the strength and fracture toughness of them[36], [40]–[45].

1.2.3.2. Electronic properties and applications

Based on Moore's law[46], metal-oxide-semiconductor field-effect transistors (MOSFETs) will reach to their geometrical limit in the near future. Electrostatic degradation and short channel effects are the major challenges in existing FETs with short gates[47], [48]. Furthermore, reducing the channel thickness of the existing silicon MOSFETs to the thickness of less than 2 nm [49]results in the reduction of their mobility[17]. Hence, the new generation of the materials will be needed to address these issues. Graphene which has a one atom thickness and mobility of up to $100000 \text{ cm}^2\text{V}^{-1}\text{S}^{-1}$

¹[50] is one of the promising 2D materials for future electronic devices, especially high-frequency ones[51]. Although graphene has a superior mobility, the absence of a bandgap makes it inapplicable in logic transistors. However, there has been some reports which have tried to change graphene band structure by making graphene nanoribbons[52], biasing bilayer graphene[53] and inducing strain to graphene[54]. None of these methods were completely successful in opening a bandgap in graphene practically. For example, making graphene nanoribbons results in the reduction of the graphene mobility due to increasing the effective mass of the charge carriers[17], [55]. Or, opening a band gap via inducing the strain into the graphene needs applying more than 20% global uniaxial strain, which is not applicable.

In radio frequency devices, such as small-signal amplifiers, switch off is not a challenging issue, which makes the use of graphene very favorable in these applications[17]. One of the important parameters in radiofrequency applications is the cut-off frequency value which strongly depends on the field effect mobility of the device. The highest reported cut-off frequency for graphene devices is 100 GHz with a gate length of 240 nm, which beat out the best silicon MOSFET results with the gate length of 550 nm[51]. This value is very impressive; although, graphene radiofrequency devices exhibit weak saturation behavior[17], [51].

1.3. Literature review of MoS₂

1.3.1. Introduction

Molybdenum disulfide is a very well-known material as a dry lubricant[56] or intercalation host[57], [58] for decades. It is a layered material consisting of Molybdenum (Mo) as a metal and Sulfur (S) as a chalcogen atom. While these atoms are covalently bonded in the in-plane direction, the inter layer bonding between them is van der Waals (vdw) bonding, resulting in having different properties in the in-plane and out-of-plane directions. For instance, it is very easy to cleavage the layers in the out-of-plane direction, while it needs a huge amount of energy to break the covalent atomic bonding in the in-plane one. After the discovery of a single layer graphene sheet by mechanical exfoliation method in 2004[10], single layer MoS₂ and other transition metal dichalcogenides (TMDs) have been produced by the same methods for fundamental studies. Other methods of production, such as chemical exfoliation[59]–[61] and chemical vapor deposition methods [62], [63], have been used to produce these material with large scale approaches. In the contrary with graphene which is chemically an inert material[8], MoS₂ is a very promising candidate as a catalyst for electrochemical hydrogen production due to its high chemical activity and stability[64]. There have been many reports and reviews on MoS₂ as a catalyst for hydrogen evolution reaction (HER)[1], [4]–[7] which shows the importance and potential of this material for the energy applications. Furthermore, single and multilayer MoS₂ have shown promising results for electronics and optoelectronics applications[65]–[67]. One major challenge in

using MoS₂ for electrical devices is the quality of the electrical contacts, which has a direct effect on the efficiency of the entire device [68]. Basically, there is a Schottky barrier between MoS₂ and metal electrodes resulting in considerably increasing the contact resistance and reducing the flow of the charge carriers into the MoS₂ devices. This critical issue influences scientists to create heterostructures such as MoS₂/Gr[1], [69], [70] or MoS₂ (1T)/MoS₂ (2H)[71] to decrease the contact resistance at the interface resulting in significantly increasing the efficiency of the devices.

1.3.2. Production methods

1.3.2.1. Mechanical exfoliation

Mechanical exfoliation is the first method which has been used for fundamental studies of the two-dimensional materials[10]. Generally, in this method the single layer of the material will be produced by multiple cleavage of the bulk of it with scotch tape. Novoselove et al.[72] published the first report on mechanically-exfoliated single-layer MoS₂. Basically, MoS₂ has three known polytypes, which are 1T, 2H and 3R based on the coordination of the Mo atoms in its crystal structure[73]. Since the bulk of the MoS₂ is 2H, exfoliated single-layer MoS₂ would also be 2H-MoS₂ with semiconducting properties. Although mechanical exfoliation methods will provide very high quality samples, there is no thickness control on the exfoliated samples and the size of the flakes produced by this method are very small. So, there is a need to produce MoS₂ by other synthesization methods for mass production applications.

1.3.2.2. Chemical exfoliation

Liquid phase exfoliation is one of the methods which has been used to produce 2D materials for mass productions. Basically, with liquid exfoliation method, the bulk of the material will dissolve in a solution with a surface tension close to the surface tension of the 2D materials. Next, the van der Waals forces between the layers of the bulk material will be broken by the aid of the sonication to produce single-layer sheets. This Direct dispersion method has also been used for production of the MoS₂ sheets, although achieving to the single-layer sheets does not have a high yield in this method[61].

Producing single-layer MoS₂ sheets by using intercalates was another method of the chemical exfoliation, which has been used by the scientist[61] a few years ago. In this method, to have a uniform dispersion of the MoS₂ layers inside of the water and weaken the van der Waals bonding between the layers[61], first, the reducing agent will be intercalated into the MoS₂ layers. Next, the intercalated MoS₂ sheets will be sonicated inside of the water or ethanol to produce single layer MoS₂ sheets. N-butyl lithium is one of the reducing reagent which has been used[61] to produce single layer MoS₂ sheets. Although the yield of single layer MoS₂ sheets is very high in this method, there is the possibility of producing the mixture of the 1T and 2H-MoS₂ single-layer sheets in this method[73]. To produce only 2H-MoS₂ by this method, scientist have been using other surfactant like sodium cholate[74], [75].

Electrochemical exfoliation is another method which has been used by scientists to produce atomically thin MoS₂ sheets. Basically, in this method as a result of the water

oxidation, the OH and O radicals weaken the van der Waals bonding by inserting between the MoS₂ layers. Then, the bulk of MoS₂ will be expanded and finally exfoliated to the single-layer sheets by the gas bubbles produced as a result of the radical oxidations[76]. This method yields achieving large single-layer MoS₂ sheets while there is the possibility of oxidation during the process, which can be treated by post-annealing[73].

1.3.2.3. Chemical vapor deposition

Liu et al.[77] has used a layer of ammonium thiomolybdate (NH₄)₂ MoS₄ for Producing large scale thin layers of MoS₂. In this method, they immersed insulating substrates such as sapphire into the solution of the dimethylformamide (DMF) and (NH₄)₂MoS₄ to coat a layer of the (NH₄)₂MoS₄ on top of the substrate. Then the coated substrate was annealed at 500 °C in the presence of the Ar/H₂ gas, which resulted in the formation of the thin layers of MoS₂. Since their Raman characterization revealed that the synthesized MoS₂ layers do not have perfect crystallinity, they performed the second annealing process at 1000 °C in the presence of the Ar/S gas to improve the crystallinity of the synthesized structures. Their second annealing process considerably improved the crystallinity of their synthesized MoS₂ structures and their field effect transistor (FET) measurements show electrical mobility of 6 cm²V⁻¹S⁻¹ and on/off ratio of the 10⁵, which were comparative with electrical characteristic of the mechanically exfoliated samples.

Deposition of a thin layer of Molybdenum (Mo) on SiO₂ substrate was another method which has been used by Zhan et al.[78] to produce thin layers of MoS₂. In this

approach, a thin layer of Mo was deposited on the SiO₂ substrate by electron beam evaporation technique. Then Mo-coated substrate and sulfur precursor were placed into the furnace at two different zones. When the temperature of the Mo-coated substrate reached 750 °C, the sulfur also vaporized to react with the Mo in order to produce thin layers of MoS₂. Their reported mobility for the grown MoS₂ samples were between 0.004 to 0.04 cm²V⁻¹S⁻¹.

Synthesizing MoS₂ by sulfurizing the molybdenum trioxide (MoO₃) is one of the most successful CVD methods for large scale single layer MoS₂ production [79]. In this method, the sulfur powder and MoO₃ powder will be used as precursors for the growth. The substrate will be placed upside down on top of the MoO₃ crucible and argon gas will be used as a carrier gas during the growth. The complete explanation of this method is provided in chapter 3.

1.3.3. Properties and applications

1.3.3.1. Electronic properties and applications

While the band gap of the bulk MoS₂ is indirect at the Γ -point, it shifts to be direct for the single-layer MoS₂[80]–[82], which is due to the quantum confinement[83]. This property makes monolayer MoS₂ very promising for electronic applications, especially high switching ones. Currently the smallest applicable FET transistors are the silicon based metal-oxide-semiconductor FETs with the feature length of the 22 nm[83]. Short-channel effects, which are the result of the quantum effects[83], make reduction size of

the conventional electronic devices challengeable and almost impossible. Hence, usage of the 2D materials like MoS₂, which have just one atom thickness, can break the scale limitation and revolutionize the size of the electronic devices. While decreasing the size of the electronic devices is very important, having high carrier mobility, high on/off ratio and low off-state conductance is also essential for high speed switching transistors[83]. The reported mobility, on/off ratio, and subthreshold swing of top gated MoS₂ are >200 cm²V⁻¹S⁻¹, 10⁸ and 74 mv respectively[67] which are promising values to satisfy the circumstances of the high speed switching transistors at very small scales. Astonishing electrical performance of the MoS₂ together with high mechanical stiffness and strength (30 times stronger than steel)[84] also makes it an encouraging candidate for flexible electronic devices. Tuning the bandgap of the MoS₂ based on its number of layers also makes it applicable for photodetection devices. It has been shown that single and double layer MoS₂ are effective for detecting the green light while its triple layer is effective for red light detection[83], [85].

1.3.3.2. Chemical properties and hydrogen evolution reaction applications

MoS₂ and other TMDs as low-cost and earth abundant materials, which show their potential for hydrogen evolution reaction, have opened up a new research direction in energy applications for scientists during recent years[7], [86]. Although the bulk of the MoS₂ is not an active catalyst for HER[87] due to catalytically inertness of its surface, MoS₂ nanostructures have shown enhanced results for HER activity[88], [89]. The density functional theory (DFT) calculations have shown that the catalytic activity of the

Mo terminated edge of MoS_2 for HER is close to the noble metals like platinum[89]. Hence, one way to enhance the catalytic activity of the MoS_2 is increasing the number of the MoS_2 active sites. Vertically oriented MoS_2 nanowires is one of the works which has been done in this field by Chen et al.[90] to increase the active surface area of the MoS_2 . In this work, diluted H_2S gas is used to react with the MoO_3 nanowires and change their shell structure to MoS_2 structure serving as active sites during the reaction. However, the core of the structures remained unchanged during the reaction. Hence, the electrons can easily transfer to the active sites through the MoO_3 core, which is a conductive material. Furthermore, the proper sulfurization temperature ($200\text{ }^\circ\text{C}$) results in the growth of the complete acid resistant MoS_2 layers around the MoO_3 core and significantly increasing the stability of the grown catalyst in the acidic media[64]. Another attempt to increase the active edge sites of the MoS_2 was synthesizing vertically aligned MoS_2 by sulfurization of the 5 nm thick Mo layer deposited on the substrate via electron-beam evaporation technique[91]. The results have shown the low catalyst activity with the overpotential of 440 mv, although the turn over frequency (TOF) was 0.013 S^{-1} , proving high activity of the edges.

The other way to improve the HER efficiency of the catalyst is decreasing the charge transfer resistance between the electrode and MoS_2 which is a semiconductor material. Making heterostructures with 2D materials can help to satisfy this demand. Shi et al.[82] have grown the heterostructure of the MoS_2 /graphene in 2012 by Thermal decomposition of the MoS_2 flakes on top of the CVD grown graphene. In this work they have not done

any electrochemical measurements, but they have suggested that the graphene can act as an electrode due to its high electrical and mechanical stability and MoS₂ flakes can serve as catalyst for electrochemical applications.

1.4. Research Objective

In this Study, a method is presented to grow the heterostructure of the 3D structured MoS₂ and Gr. The graphene film is first grown by an APCVD method and then transferred on top of the glassy carbon substrate. Next, the 3D structured MoS₂ is grown on top of the Gr/glassy carbon substrate using another APCVD approach. Different experiments and characterizations are performed to understand the growth mechanism of the 3D structured MoS₂ and electrochemical experiments are performed to measure the HER activity of the grown catalyst with and without the graphene film. Density Functional Theory is also carried out to find out the catalytic properties of the MoS₂ and the effect of Gr. It is worth nothing that synthesizing 3D structured MoS₂ is significantly improved the HER activity of it. Also, the growth of this structure on top of the graphene film results in considerably enhancing the charge transfer from the electrode to the catalyst.

CHAPTER 2: Synthesize and Characterization of CVD MoS₂/Gr Heterostructure

(Most of this chapter is entirely copied from my published paper with the following citation:

A. Behranginia, M. Asadi, C. Liu, P. Yasaei, B. Kumar, P. Phillips, T. Foroozan, J. C. Waranius, K. Kim, J. Abiade, R. F. Klie, L. A. Curtiss, and A. Salehi-Khojin, “Highly Efficient Hydrogen Evolution Reaction Using Crystalline Layered Three Dimensional Molybdenum Disulfides Grown On Graphene Film,” *Chem. Mater.*, p. acs.chemmater.5b03997, 2015. Please refer to the authors’ contributions in page iv in the beginning of this document for details of my contributions)

2.1. Introduction

Recently, MoS₂ is being widely used in a broad range of applications from electronics[67], [92] and optoelectronics[93], [94] to energy conversion[95], [96] and storage systems[97]. Although enormous attention has been dedicated to produce atomically thin two dimensional (2D) MoS₂ films,[62], [76]–[78], [98], [99] layered three dimensional (3D) structures of MoS₂ with a high density of active edge atoms for electrochemical applications have not yet been explored.

To date, several synthetic structures, such as MoS₂ nanoparticles on Au (111) [88], vertically aligned MoS₂ nanoflakes[91], ordered double-gyroid MoS₂ bi-continuous networks[96], defect-rich MoS₂ nanosheets[100], and chemically synthesized thiomolybdate [Mo₃S₁₃]²⁻ clusters[101] with sulfided Mo edge atoms have been developed and tested for HER. In this report, we employed the chemical vapor deposition method to synthesize crystalline 3D structured MoS₂ with bare Mo edge atoms on graphene film, and demonstrate its outstanding activity and stability for HER. In particular, the electrochemical impedance spectroscopy (EIS) experiments and density

functional theory (DFT) calculations reveal that Mo edge terminated MoS₂ and graphene show strong synergy for HER resulting in significant enhancement in the electron transfer to the reactants and desorption of intermediates from catalyst surface.

2.2. Material Synthesis and characterizations

2.2.1. CVD graphene Synthesis procedure and characterizations

The three zone MTI CVD furnace (model OTF-1200X) with the added oil trap at the exhaust of the system was utilized to grow graphene film. Adding oil trap is to prevent the oxygen gas from diffusing back into the system during the growth procedure. The graphene film was grown on top of the copper foil, purchased from Alfa Aesar Company (product no. 46365). Before the growth, the copper foils were immersed inside of the 10% diluted Hydrochloric acid (HCL) solution for 15 minutes to remove any oxidation from the copper surface. Next, they were rinsed with Aceton and Iso Propanol (IPA) and dried with nitrogen (N₂) flow. Then, the foils were placed into the 3.14” quartz tube and the furnace is evacuated to ~ 1 *mTorr* to remove unwanted gases from the system. The system was kept at vacuum pressure for 15 minutes and then it was pressurized to the atmospheric pressure with flowing the Argon (Ar) gas. The temperature of the furnace is increased to 1050 °C in 60 minutes while the diluted H₂ and Ar gases was flown inside of the furnace with 165 sccm and 175 sccm respectively. Then the furnace was kept at this temperature for 60 and 90 minutes to grow partially covered graphene flakes and fully covered graphene film in that order. During this step 15 sccm methane gas is also flown to provide the carbon source for the graphene growth. Finally, the furnace is cooled down

to the room temperature by force cooling. During the force cooling process, Ar and H₂ gases were still flown. Figure 1 show the SEM images of the partially covered graphene flakes and fully covered graphene films. These images are acquired by the In-lense detector of a Carl Ziess electron microscope integrated in a Raith e-LiNE plus electron beam lithography system at 20 kV acceleration voltage and 10 mm working distance.

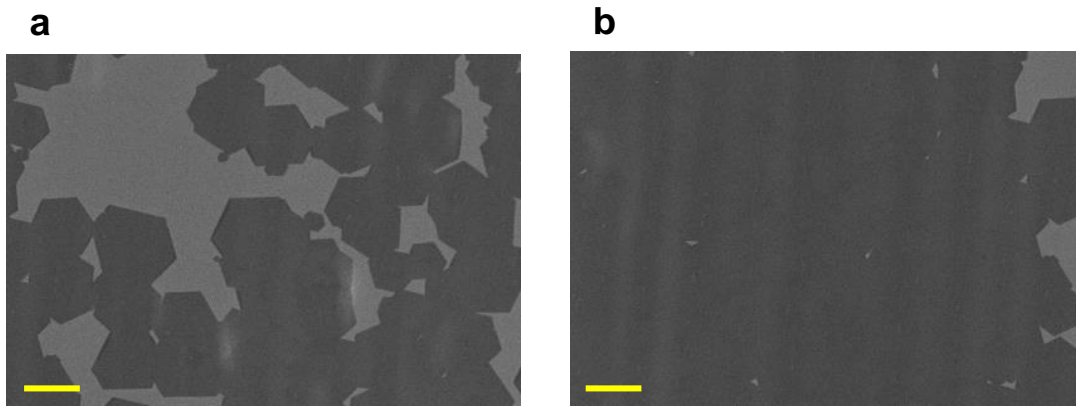


Figure 1: SEM characterization of CVD graphene. (a) Partially covered graphene flakes. **(b)** Fully covered graphene film (scale bars 20 μm).

The Acton TriVista CRS confocal Raman with 11 mw power and 0.5 μm spot size was utilized to get Raman spectra from the grown structures. The obtained Raman point spectra from the grown graphene flakes (figure 2) indicates I_G and I_{2D} Peaks which are the representative peaks of the graphene flakes. The ratio of these peaks (I_{2D}/I_G) illustrates the number of the graphene layers[102] which in this case represents that the grown graphene flakes are single layer flakes.

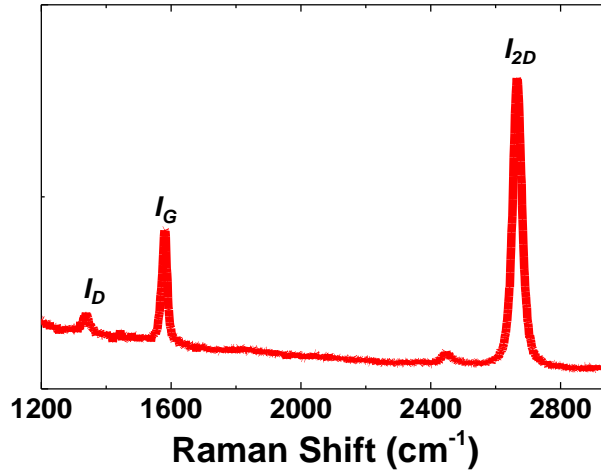


Figure 2: Raman characterization of CVD graphene. Raman spectrum with a 514.5 nm excitation laser wavelength obtained from single-layer graphene flakes.

2.2.2. CVD 3D Structured MoS₂ Synthesis procedure and characterizations

The 3D structured MoS₂ was synthesized through a dual precursor CVD method with two separated zones to precisely control the temperature profile of the growth process. Two alumina crucibles, one containing 7 milligrams of MoO₃ powder (Sigma-Aldrich, 99.98%) and the other containing 1 gram of sulfur powder (Sigma-Aldrich, 99.98%) were used as precursors for MoS₂ growth. The sulfur crucible was placed in the upstream of the furnace where the maximum temperature reached 300°C, while the MoO₃ crucible was located in the center of the tube with a maximum temperature of 850°C. The MoO₃ powder was uniformly dispersed inside of the crucible to produce a uniform concentration of MoO₃ vapor all over the target substrate which was loaded upside down on top of the MoO₃ crucible. Prior to running the temperature profile, the chamber was first evacuated down to 1 mtorr and then purged by argon flow to reach the

atmospheric pressure. During the growth process in atmospheric pressure, 200 standard cubic centimeter (sccm) of argon gas flowed in the chamber. In order to grow the 3D structured MoS₂, independent two-stage temperature profiles (Figure 3) were applied to each zone to synchronize the evaporation time of the S and MoO₃ powders to avoid the formation of intermediate structures. In more detail, the sulfur evaporation rate was sharply increased from 100°C to 300°C with rate of 10°C/min as soon as the temperature of the central zone reached 720°C. Afterwards, the central temperature was ramped up to 850°C and was kept constant for 15 minutes. Finally, the furnace was cooled down to room temperature by natural air convection. During the cool down process, the sulfur evaporation continued for about 10 minutes after the MoO₃ evaporation had stopped.

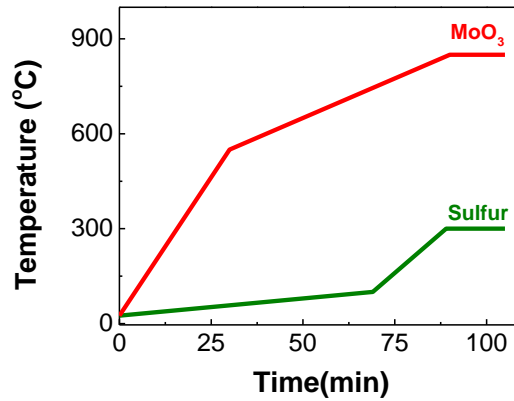


Figure 3: CVD MoS₂ temperature profile. Temperature profile for MoO₃ and sulfur zone

Figure 4a shows the low magnification SEM image of the 3D MoS₂ structures. The atomic structure of the 3D MoS₂ and its edge structure is also characterized by STEM and shown in Figure 4b. The STEM characterization was performed on a JEOL JEM-ARM200CF, operated at 200 kV, equipped with an Oxford X-Max^N 100TLE silicon

drift detector (SDD) for energy dispersive X-ray (EDX) analysis. The results exhibit a multi-layered stacking of MoS₂ nanosheets with Mo terminated edges along the (100) and (010) crystallographic planes which is similar to the previously reported edge terminations in mechanically exfoliated MoS₂. [103] The corresponding fast Fourier transforms (FFTs) taken from a multi-layered area (inset of Figure 4b) shows sharp hexagonal benzene-like patterns indicative of highly crystalline 3D structures with epitaxial stacking of the MoS₂ layers.

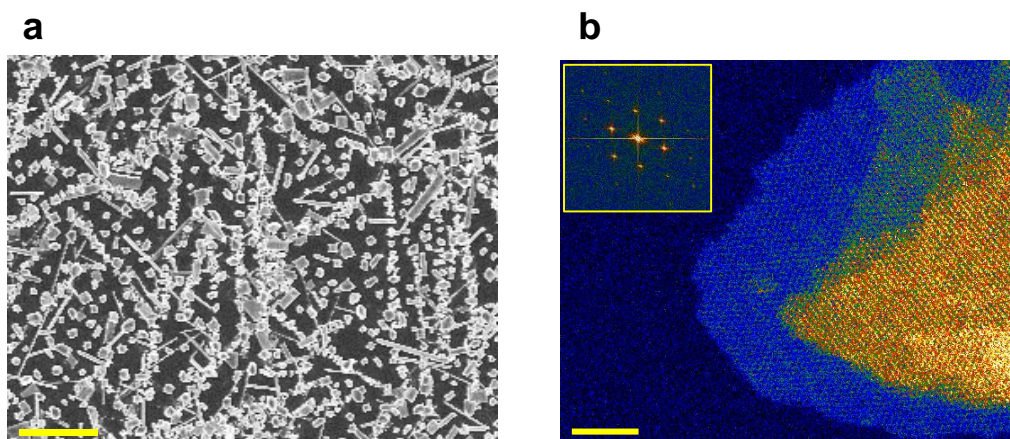


Figure 4: SEM and STEM characterization of the 3D structured MoS₂. (a) Low magnification SEM image from 3D structured MoS₂ (scale bar is 15 μm). (b) Atomic-resolution ADF STEM image, showing the layered structure of the 3D crystals (scale bar is 3 nm). The inset shows the fast Fourier transform (FFT) obtained from the multilayer region in which the unique hexagonal pattern of MoS₂ crystal implies the epitaxial stacking of the layers.

X-ray Photoelectron Spectroscopy (XPS) Analyses were performed on a monochromatic Al K α source instrument (Kratos, Axis 165, England) operating at 12 kV and 10 mA, for an X-ray power of 120 W. Spectra were collected with a photoelectron

takeoff angle of 90° from the sample surface plane, energy steps of 0.1 eV, and a pass energy of 20 eV for all elements. All spectra were referenced to the C1s binding energy at 284.6 eV. The XPS results from the 3D structured MoS_2 (Figure 5a) show standard Mo $3d_{5/2}$ (~ 229.0 eV) and S $2p_{3/2}$ (~ 162 eV) peaks consistent with the presence of Mo^{IV} and the S^{2-} present in MoS_2 structures. The XPS spectrum without any peaks at ~ 236 (a characteristic for Mo^{VI}) illustrates the absence of molybdenum oxides[104]. In addition, Figure 5b demonstrates Raman point spectra obtained from the 3D MoS_2 structure up to 800 cm^{-1} . Results indicate that MoS_2 characteristic peaks associated with E_{2g} and A_{1g} vibrational modes for 3D structured MoS_2 [105] without any other peaks up to 800 cm^{-1} which further supports the absence of oxides formation[62], [106].

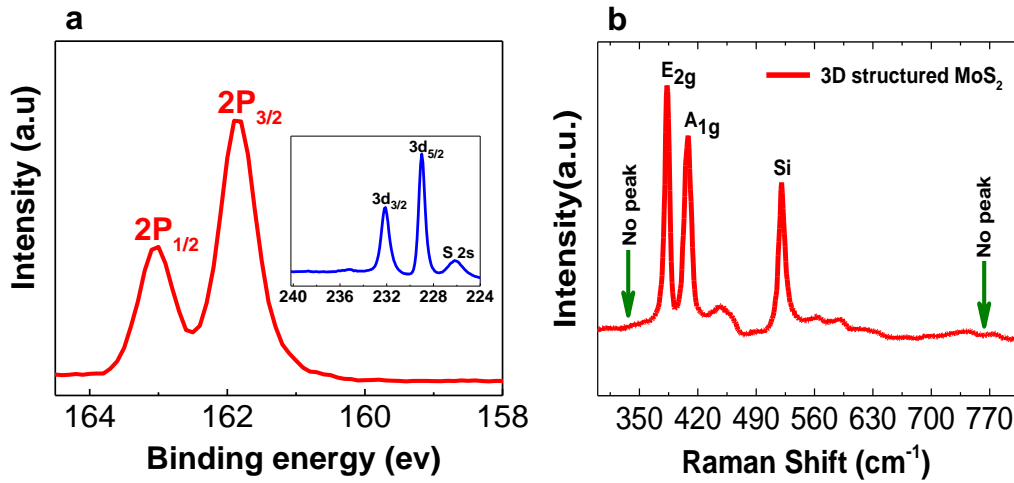


Figure 5: XPS and Raman characterization of the 3D structured MoS_2 . (a) XPS spectra of the 3D MoS_2 structure showing sulfur peak (Mo peak is shown in the inset).[104]. (b) Raman Spectra from 3D structured MoS_2 .

The obtained EDX results (Figure 6) from the 3D structured MoS_2 also reveal an

approximate composition of 32% Mo and 68% S, which is consistent with the stoichiometric ratio of MoS₂. [107]

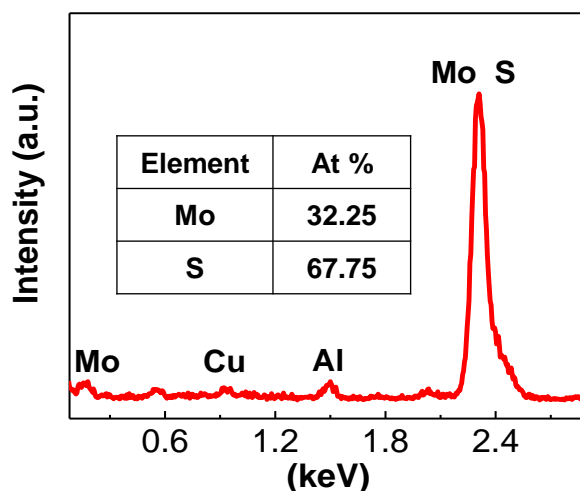


Figure 6: EDX characterization of 3D structured MoS₂. Representative EDX spectrum of MoS₂ flakes. Inset: atomic percentage of the molybdenum and sulfur which is extracted from deconvolution of the molybdenum and sulfur EDX peak.[79]

In order to visualize the layered construction of the CVD grown 3D MoS₂, we quenched the CVD chamber by force cooling to rapidly reduce the temperature and terminate the growth of the top layers. High magnification SEM images of the resulting structure (Figure 7) not only show the layered construction of the 3D grains, but also reveal an epitaxial conformance between the layers, as evidenced by the parallel edges in the stacked layers. This is consistent with the FFT patterns of the atomic resolution images obtained from STEM.

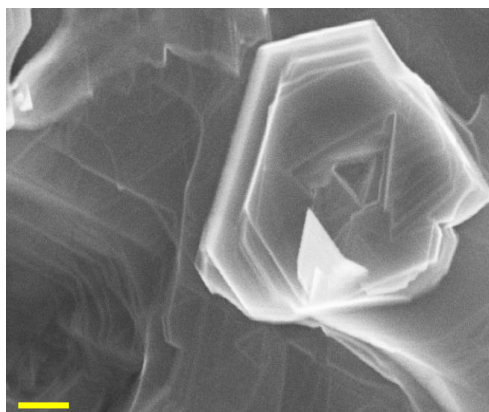


Figure 7: SEM characterization of 3D structured MoS₂. SEM image of the 3D structured MoS₂ from a rapid cooling experiment (scale bar is 0.5 μ m).

To gain insight into the growth mechanism of the 3D MoS₂, we deliberately placed MoO₃ powder (2.5 mg) in the corner of the crucible (Figure 8a) to visualize the transition from 2D to 3D MoS₂. An optical image of the grown structure on a Si/SiO₂ substrate is shown in Figure 8b. Variation in the color spectrum of the sample corresponds to different concentrations and morphology of the MoS₂ structures. Detailed morphological characterization was performed by optical and scanning electron microscopy (SEM) as shown in Figure 8c, in which the concentration increases as one moves from left to right. Starting from the low concentration side, initially small triangular MoS₂ monolayer flakes appear on the substrate (Figure 8c-1). As the concentration increases, the flakes grow to larger sizes with some smaller MoS₂ islands growing on top of the flakes (Figure 8c-2). As shown in Figure 8c-3, the flakes keep growing in size, reaching together and making grain boundaries, meanwhile smaller MoS₂ islands begin to grow in the out-of-plane direction on top of the existing flakes. Next, the existing islands merge together

and eventually form a polycrystalline film with numerous islands of multilayer MoS₂ (Figure 8c-4). In higher concentration regions (Figure 8c-5), white lines representing thicker MoS₂ structures appear on the polycrystalline film, which are believed to form due to higher local growth rate on the defect sites such as grain boundaries[108]. Moving to even higher concentration regions (Figure 8c-6), the grown structures rapidly convert to 3D granular structures with a high surface roughness and spatial heterogeneity. This abrupt and localized transition from the 2D to 3D structures resembles the Stranski-Krastanov (SK) growth mechanism of thin films, in which the growth mode suddenly changes as the layer thickness exceeds a critical level[108]–[111]. One possible explanation of such sudden transition can be the release of a residual strain induced by thermal and intrinsic stresses between the MoS₂ and the substrate.

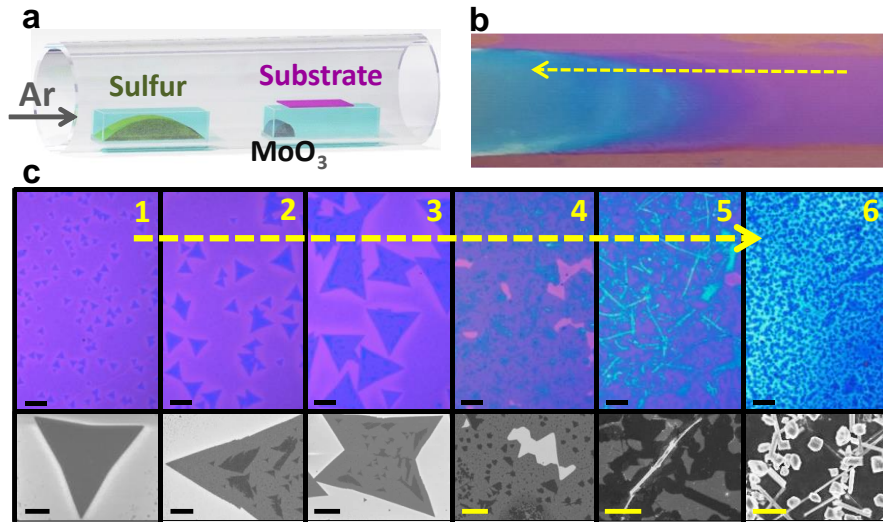


Figure 8: MoS₂ CVD setup, Optical and SEM characterizations of the different structures of MoS₂. (a) Schematic of the MoS₂ CVD setup. (b) Optical image of the grown structure on a

Si/SiO₂ substrate. (c) Detailed optical and SEM images of MoS₂ structures shown in b from right to left. (Scale bars in all optical images are 30 μm and in SEM images are 2, 15, 15, 10, 4, 4 μm from left to right, respectively).

To test this hypothesis, we performed Raman spectroscopy on the grown structures from monolayers to 3D structures (Figure 9). Interestingly, we observed that the peak positions of our multilayer films have 3 cm^{-1} positive shift relative to the bulk spectrum. This shift of spectrum is known to be indicative of an induced strain in the grown structure.[112] However, the peak positions of the 3D structured MoS₂ shift back to the peak positions of the bulk MoS₂, which implies the release of the induced strain. Here, we note that the difference in the positions of the E_{2g} and A_{1g} peaks is known to be dependent on the thickness of the MoS₂ structure[105] which is changing from $\sim 20 \text{ cm}^{-1}$ in single layer to $\sim 25 \text{ cm}^{-1}$ in our multilayer and 3D structures. This is independent of the observed blue shift in the multilayer spectra, which is due to the induced strain.

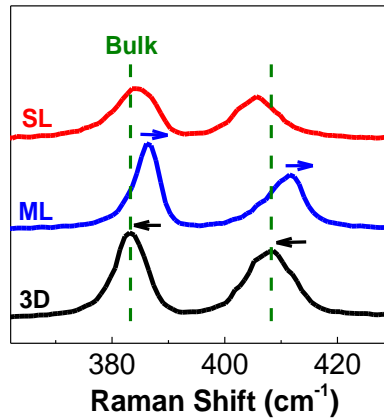


Figure 9: Raman characterization of MoS₂ from single-layer to 3D structure. Raman point spectra obtained from a monolayer flakes (red), multilayer MoS₂ film (blue) and 3D structured MoS₂ (black).

Based on above discussions, we propose a dual-step Stranski-Krastanov mode for the growth of 3D MoS₂. First, growth initiates from grain boundaries or ordered defects that have high surface energies. Next, the 3D structures form on the film with the thickness beyond the critical point in a less or more compact manner depending on the concentration of Mo and S (Figure 10).

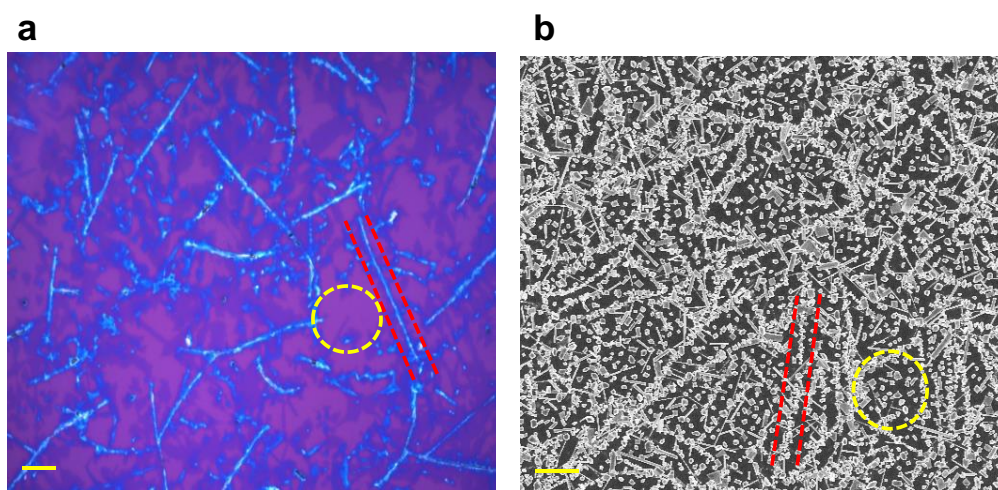


Figure 10: Optical and SEM characterization from 3D structured MoS₂. (a) Optical image of multilayer MoS₂ film from the region in which the 3D growth has not yet initiated. (b) SEM image of the region where the 3D growth is just initiated. Line type highly compact patterns of 3D MoS₂ grains similar to the topography of the grain boundaries represents that growth is favorable on the grain boundaries compared with the central parts of the MoS₂ layers (scale bars are 15 μ m).

We also synthesized uniform 3D MoS₂ on (i) amorphous glassy carbon (GC), (ii) graphene covered GC and (iii) Si/SiO₂ substrate (transferred to GC for electrochemical experiment). The glassy carbon and graphene substrates are intentionally selected due to their high conductivity, inert nature and wide applicability in various electrochemical

systems[95], [113]. For easier characterization, we initially synthesized MoS_2 on partially covered graphene flakes, which was then transferred to Si/SiO_2 . The SEM image of the directly grown 3D structures (Figure 11) illustrates that the growth is more compact on top of the hexagonally shaped graphene flakes compared to the bare Si/SiO_2 substrate. This is attributed to the presence of wrinkles and defects on graphene film which act as nucleation sites and accelerate the growth rate of the 3D structures[114]. It is worth mentioning that here we used partially covered graphene flakes to show the difference of the growth on top of graphene flakes compared to the bare Si/SiO_2 substrate and fully covered graphene film is used for electrochemical experiments.

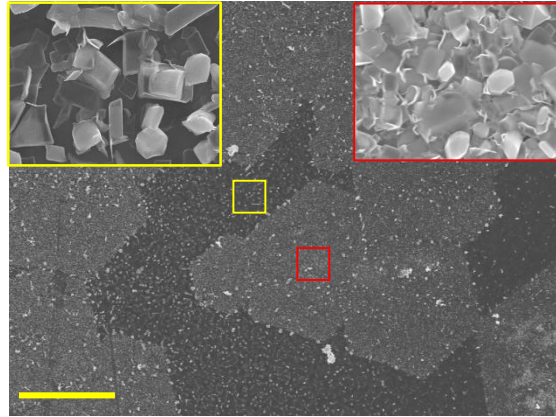


Figure 11: SEM characterization of 3D structured MoS_2 grown on graphene flakes and bare substrate. SEM image of the 3D structured MoS_2 directly grown on top of partially covered graphene flakes transferred on SiO_2 substrate (scale bar is 20 μm). The insets magnify the 3D MoS_2 in same image as indicated by yellow (bare SiO_2 substrate) and red (on top of graphene flakes) squares.

Figure 12 shows the Raman spectra of the 3D structured MoS_2 on graphene film. The presence of the G and 2D characteristic peaks of graphene together with the A_{1g} and

E_{2g} peaks in the Raman spectrum confirms the growth of 3D MoS_2 on top of the graphene flakes.

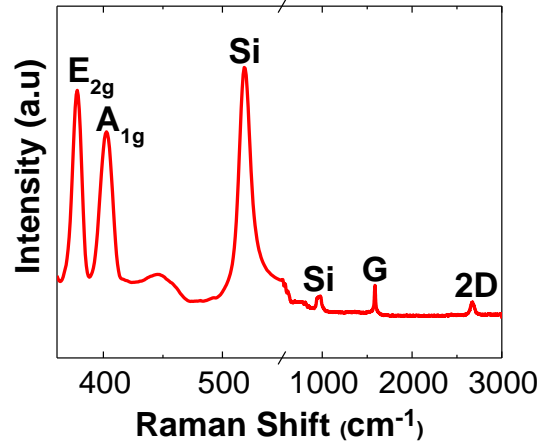


Figure 12: Raman characterization of 3D structured MoS_2/Gr heterostructure. Raman spectra of 3D MoS_2 on top of graphene film with the G and 2D characteristic of graphene and the A_{1g} and E_{2g} peaks of MoS_2 .

2.3. Conclusion

An APCVD method is used to grow the 3D Structured MoS_2 directly on CVD graphene. This method of synthesization allows for the large size, time and cost effective mass production of this heterostructure for industrial applications. The characterization confirmed the layered construction of the 3D Structured MoS_2 which can provide many active edges for chemical reactions. Also, performing control experiments reveals that the growth of the 3D Structured MoS_2 follows the Stranski-Krastanov growth mode in which the transition from 2D to 3D growth will happen after reaching to the critical thickness.

Chapter3: Electrochemical experiments and DFT calculations

(Most of this chapter is entirely copied from my published paper with the following citation:

A. Behranginia, M. Asadi, C. Liu, P. Yasaei, B. Kumar, P. Phillips, T. Foroozan, J. C. Waranius, K. Kim, J. Abiade, R. F. Klie, L. A. Curtiss, and A. Salehi-Khojin, “Highly Efficient Hydrogen Evolution Reaction Using Crystalline Layered Three Dimensional Molybdenum Disulfides Grown On Graphene Film,” *Chem. Mater.*, p. acs.chemmater.5b03997, 2015. Please refer to the authors’ contributions in page iv in the beginning of this document for details of my contributions)

3.1. Experimental details and results

Cyclic voltammetry (CV) experiments are carried out for these catalysts and compared with platinum which is the most efficient catalyst known for HER. All experiments are performed at identical conditions using 0.5 M H₂SO₄ as the electrolyte. The current densities are normalized with respect to the geometrical surface area and reported based on RHE (reference hydrogen electrode) scale. As shown in Figure 13a, both MoS₂ on SiO₂ (transferred to GC) and directly grown on GC exhibit low onset potentials of 175 and 140 mV, respectively. Interestingly, the HER takes place at a much smaller onset potential (70 mV vs RHE) for the MoS₂ on graphene sample. In particular, 10 mA.cm⁻¹ current density is achieved at ~100 mV overpotential. A similar HER current density was recorded at ~180 mV overpotential for the recently studied efficient thiomolybdate clusters.[101]

Additionally, the linear part of Tafel plot for three different catalysts was studied to further explore their catalytic properties and HER mechanisms.^{5,17} In general, three elementary reaction steps that can control the rate of HER are: (i) adsorption of reactant

(H⁺) on catalyst active sites (Volmer step), (ii) intermediate formation (H_{ad}, Tafel step), and (iii) product desorption (Heyrovsky step) from active sites.^{25–27}



Tafel slopes of 120, 40, and 30 mV.dec⁻¹ are correlated to Volmer, Heyrovsky and Tafel step, respectively, as a rate determining step (RDS) for HER.²⁷ The obtained Tafel slope and exchange current density for different studied catalysts are shown in Table 1 and Figure 13b. The Tafel slope for MoS₂ on graphene is ~41 mV.dec⁻¹ proposing the Volmer-Heyrovsky (rxn 1 and 2) as a dominant mechanism and Heyrovsky step as a RDS[95], [101], [115]–[117]. Tafel slope for MoS₂ on GC (~55 mV.dec⁻¹) and transferred MoS₂ (~68 mV.dec⁻¹) also suggest similar mechanism with Heyrovsky step as a RDS. However, the calculated lower Tafel slope (~41 mV.dec⁻¹) and higher exchange current density (18.2 μA.cm⁻²) for the MoS₂ on graphene (Table 1) implies a remarkable improvement in the charge carrier mobility of the MoS₂.

Table 1: Extracted exchange current density for different tested catalysts: Extracted exchange current density of MoS₂ grown on graphene, MoS₂ grown on GC and MoS₂ transferred to GC compared with Pt.

Catalyst	Intercept at $\eta = 0$	Exchange current density (A.cm ⁻²)
MoS ₂ grown on graphene	-4.74	1.82×10^{-5}
MoS ₂ grown on GC	-4.95	1.12×10^{-5}
MoS ₂ transferred to GC	-5.92	1.2×10^{-6}

To further explore the reaction mechanism and effect of graphene in catalytic performance of MoS₂, we performed binding energy measurement in 0.1M perchloric acid (HClO₄) solution at potential ranging from -0.1 to 0.4 V vs Ag/AgCl with the scan rate of 10 mV.s⁻¹ (Figure 13c). In principal, a lower over-potential corresponds to a higher binding energy at the constant current density[118], [119]. The binding energy measurement shows strong adsorption (lower over-potential) for Pt compared to MoS₂ on graphene suggesting intermediate formations (Tafel step) as a RDS. This is consistent with Tafel slope of 33 mV.dec⁻¹ measured for Pt (Figure 13b). However the desorption peak shows opposite trend where MoS₂ on graphene exhibits higher desorption energy compared to Pt and MoS₂ on GC. This further verifies the Heyrovsky step as a RDS where desorption of the produced species from the catalyst surface is known to be the rate determining step for the reaction[95], [101], [115]–[117]. Furthermore, the binding energy experiment shows strong adsorption and desorption (lower over-potential) for MoS₂ in presence of graphene. We attribute this to an enhanced contact resistance between graphene and MoS₂[82], [117], [120] which could boost electrons transfer toward active edge sites.

We also performed electrochemical impedance spectroscopy experiments to study the charge transfer resistances (R_{ct}) in the MoS₂ catalyst with and without the graphene layer. In more detail, EIS experiments were performed inside the three-electrode electrochemical cell comprised of synthesized catalysts i.e., MoS₂ grown on graphene and MoS₂ grown on GC as a cathode, platinum (Pt) gauze 52 mesh (purchased via Alfa

Aesar) as the anode and Ag/AgCl (3M KCl, purchased from BASF) as the working electrode. The 0.5 M H₂SO₄ electrolyte was bubbled with pure H₂ (99.99%) during the EIS experiments. The Nyquist plots were recorded at overpotential of 150 mV to ensure that the HER takes place on both catalysts (Figure 13d). An equivalent Randles circuit model was applied to calculate R_{ct} value for each system (inset of Figure 13d). The MoS₂ on graphene exhibits much smaller R_{ct} (~65Ω) compared to that of without graphene layers (>150Ω).

Also, the Nyquist plot for different over-potentials e.g., 100, 150, 200 and 250 mV were recorded at a small (10 mV) AC voltage amplitude (to avoid the nonlinearity) and over a frequency range of 1 to 10⁵ Hz using a Voltalab PGZ100 potentiostat. Figure 14a and b show the recorded Nyquist plots at different over potentials for MoS₂ grown on graphene and GC during HER. Results indicate a smaller charge transfer resistance [95], [121] at all over-potentials due to enhanced contact between MoS₂ and graphene further supporting the results of binding energy measurements.

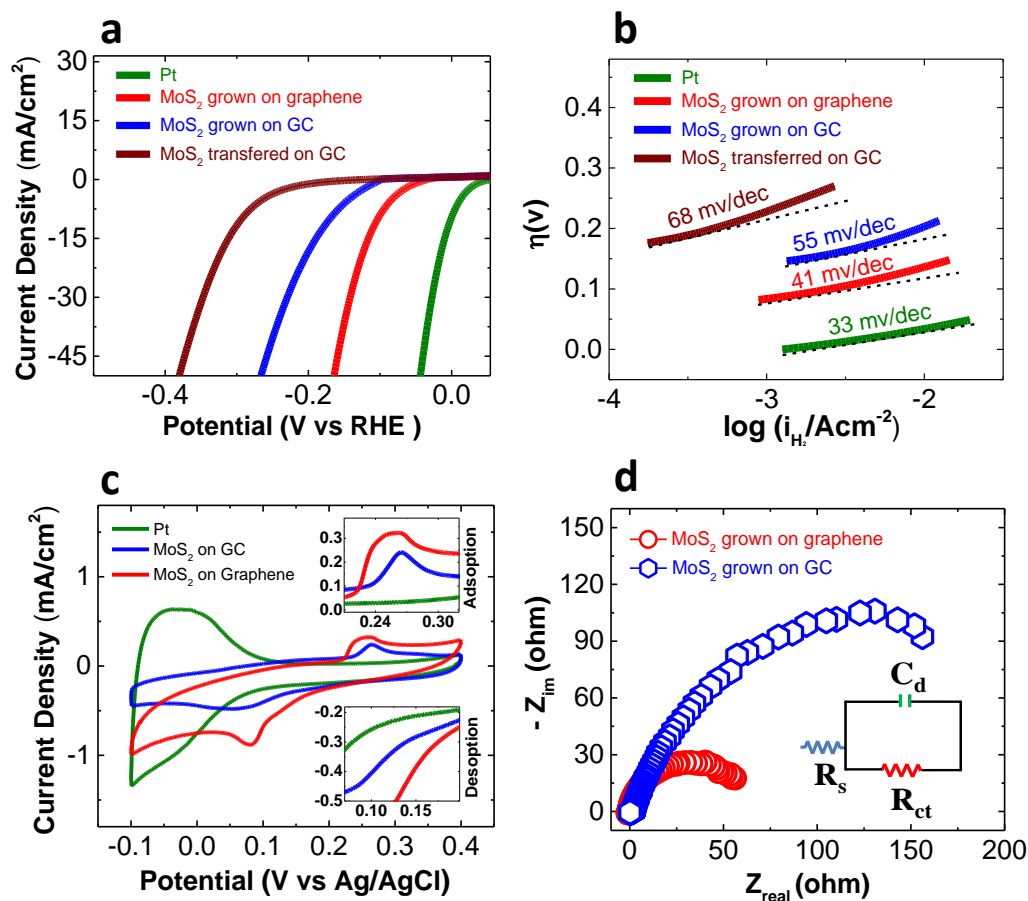


Figure 13: CV, TOF, Binding energy and Nyquist measurements. (a) Cyclic voltammetry curve for Platinum, MoS₂ grown on graphene, grown on GC and Transferred to GC. (b) Tafel plot obtained for different catalysts. 3D MoS₂ grown on graphene shows lower Tafel slop than that of grown on GC or grown on Si/SiO₂ and transferred on GC. (c) Binding energy measurement for Pt, MoS₂ on graphene and GC in 0.1M HClO₄ solution. The results confirm higher adsorption and desorption energy for MoS₂ on graphene at the constant current density compared to direct grown MoS₂ on GC. (d) Nyquist plots collected from EIS experiments at overpotential of 150 mV for 3D MoS₂ grown on graphene and GC, evidencing higher charge transfer rate for 3D MoS₂ grown on graphene. An equivalent Randles circuit was fitted to the data to calculate R_{ct} value for each catalyst system (inset).

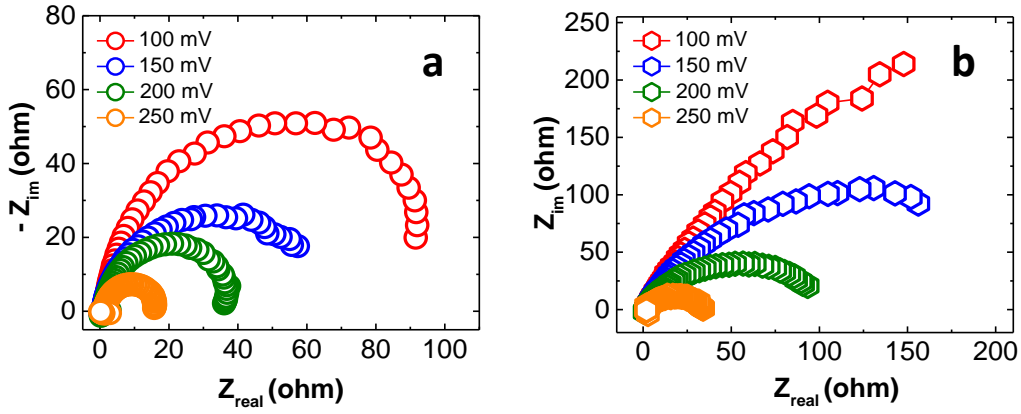


Figure 14: EIS measurements. EIS results for MoS₂ grown on (a) graphene covered GC, (b) GC substrate at different over-potentials. The Recorded Nyquist plot clearly shows the low charge transfer resistance (R_{ct}) of MoS₂ grown on graphene catalyst at all over-potentials resulting in a much faster electron transfer during HER.

The turnover frequency is also calculated for different MoS₂ catalysts using the roughness factor (RF) method[96]. The RF number of our catalyst is determined by comparing the double layer capacitor (C_{dl}) of this catalyst with flat standard MoS₂ (60 $\mu\text{F}\cdot\text{cm}^{-1}$). The CV experiment at different scan rates was used to calculate the C_{dl} of catalysts[122] (Figure 15a). The extracted C_{dl} values from the slope of current density-scan rate graphs at +0.2 V (Figure 15b) are equal to 2.13 and 1.68 $\text{mF}\cdot\text{cm}^{-1}$ for MoS₂ on graphene and GC, respectively. The calculated number of active sites for MoS₂ on graphene (4.07×10^{16} sites. cm^{-2}) is ~ 1.2 times higher than those of amorphous GC (3.21×10^{16} sites. cm^{-2}).

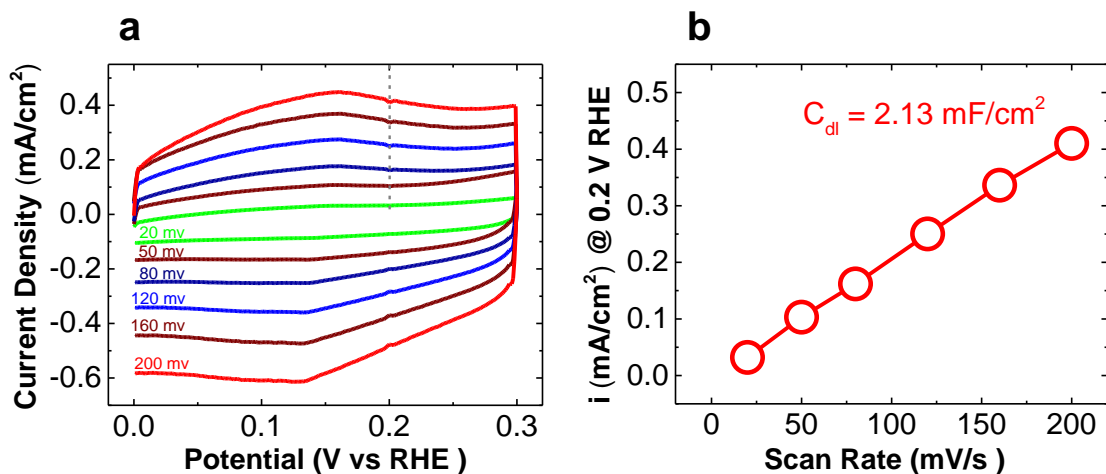


Figure 15: Electrochemical measurements. Electrochemical measurement for determining TOF: (a) a cyclic voltammetry (CV) curve of MoS₂ grown on graphene at different scan rates. The experiment was performed at 0.5 M H₂SO₄ electrolyte by sweeping potential between 0 to +0.3 V vs RHE (non-faradic region). (b) Current density of CV experiment at overpotential +0.2 V vs RHE as a function of scan rates. The slope of this line shows double layer capacitor for MoS₂ grown on graphene catalyst system (2.13 mF.cm⁻²).

Moreover, the calculated TOFs for MoS₂ on graphene show higher values at entire range of overpotentials (Figure 16a). In particular, TOF at 200 mV overpotential is > 4 (s⁻¹) which suggest a remarkable activity of the catalyst for HER.

The stability of the MoS₂/ graphene catalyst was studied during 1000 continues cycles of CV experiment. The cycles were performed between 0.1 V and -0.2 V with 100 mV.s⁻¹ scan rate. The magnetic stirring system and continuously bubbling of pure H₂ (99.99%) inside the solution were applied to eliminate mass transfer effect during the stability experiment. As shown in Figure 16b, approximately 5% current density decay at the over-potential of 0.15 mV confirms high stability of this catalyst during HER.

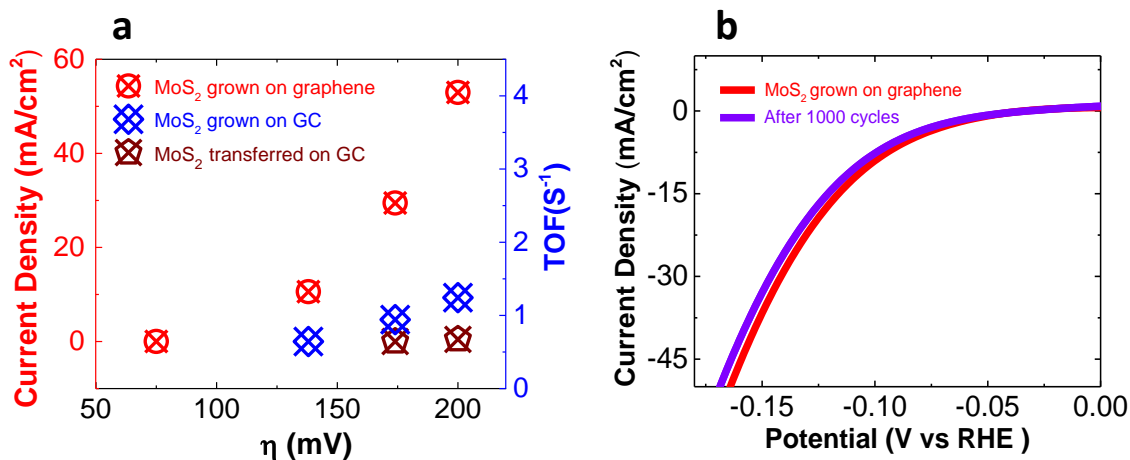


Figure 16: TOF at different current density and stability Tests. (a) Calculated TOF at different current densities with respect to the over-potentials smaller than 200 mV. (b) Stability of MoS₂ grown on graphene after 1000 continues CV cycles. This catalyst shows negligible shift (< 5%) of current densities for increased potential cycling.

3.2. Density functional theory details and results

Density functional theory calculations were carried out to study the catalytic properties of MoS₂ and the support effect. Periodic DFT calculations were performed with plane wave basis sets in VASP package[123], [124]. Single-layer nanoribbons of the MoS₂ with zigzag edges were used to truncate the 3D MoS₂ structures in the experiments for the reaction free energies and density of states (DOS) calculations. Each unit cell includes 3×4 (total 12) Mo atoms and 24 S atoms, containing both the Mo and the S edges (Figure 17a).

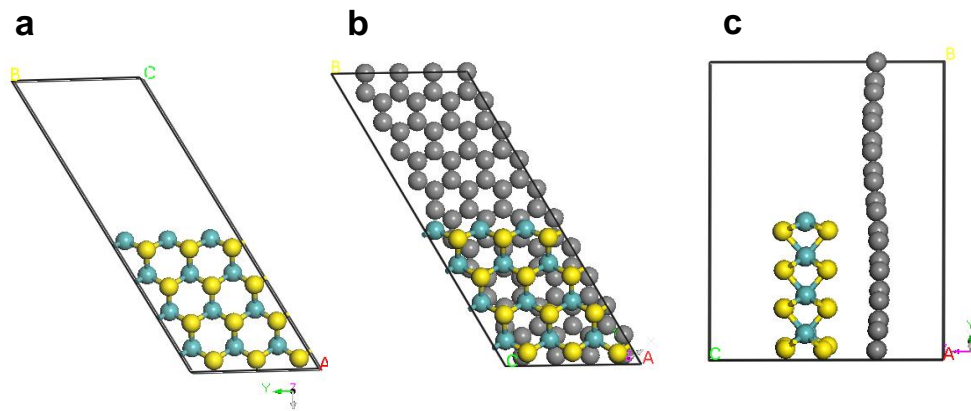


Figure 17: Atomic configuration. Structures of (a) MoS₂ nanoribbon (b) and (c) MoS₂/Graphene.

A 10 Å vacuum space is set both on top of the metal edge and between two nanoribbon periodic images. All the atoms in the MoS₂ nanoribbon were allowed to relax, while the cell shape and volume were kept fixed. For graphene supported MoS₂, the unit cell contains a 3×4 MoS₂ nanoribbon on a graphene sheet containing 4×10 graphene rings (Figure 17b). The atoms, the shape and the volume of the unit cell were allowed to be relaxed. A kinetic energy cutoff of 400 eV was used for all the calculations. K-points grids of $3 \times 1 \times 1$ and $3 \times 3 \times 1$ were used for the energy calculations of the MoS₂ nanoribbon and MoS₂/Graphene, respectively. On the other hand, K-points grids of $6 \times 1 \times 1$ and $6 \times 6 \times 1$ were used for the DOS calculations of the MoS₂ nanoribbon and MoS₂/Graphene, respectively. Γ -point was used for gas phase molecules. All the calculations with the nanoribbons are spin-polarized calculations.

After optimizations, the planar structure of the graphene became curved in MoS₂/Graphene (Figure 17c), due to the strong adhesion of the Mo edge and graphene. The PDOS of the d electrons of the Mo edge atoms on both MoS₂ and MoS₂/Graphene were calculated (Figure 18).

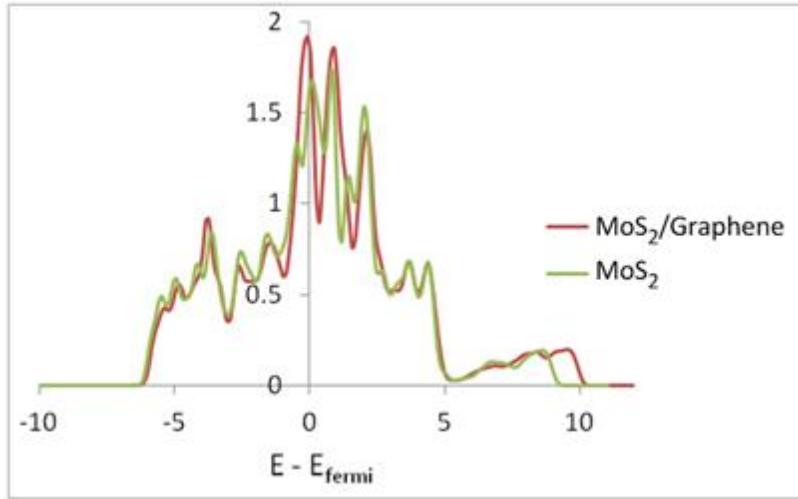


Figure 18: PDOS graph. Partial density of states (PDOS) of the d electrons of the edge Mo atoms of MoS₂ and MoS₂/Graphene

The results showed that the PDOS of MoS₂/Graphene is slightly higher at the fermi level than that of MoS₂. The hydrogen adsorption free energies were then calculated using the optimized MoS₂ and MoS₂/Graphene. In the calculations of the binding energies, we introduced the coverage of hydrogen [125] as a fraction of a monolayer (ML) with respect to the number of Mo edge atoms:

$$\theta_H(\text{ML}) = n_H / (m \text{ edge Mo atoms})$$

The binding energy of hydrogen was calculated by

$$\Delta E_H = [E (n_H \text{ adsorbed on the surface}) - E (\text{surface}) - 0.5n E(H_2)]/n$$

and the binding free energy was calculated by

$$\Delta G_H = \Delta E_H + \Delta E_{ZPE} - T\Delta S_H$$

where ΔE_{ZPE} is the zero-point energy difference between the adsorbed state of the system and the gas phase state and ΔS_H is the entropy difference between the adsorbed state of the system and the gas phase standard state (300 K, 1 bar). The entropy of hydrogen adsorption was approximated as $\Delta S_H \approx 1/2(S_{H_2}^\circ)$ where $S_{H_2}^\circ$ is the entropy of gas phase H_2 at standard conditions[125]. The results showed that the hydrogen binding free energies are sensitive to the hydrogen coverage (Figure 19).

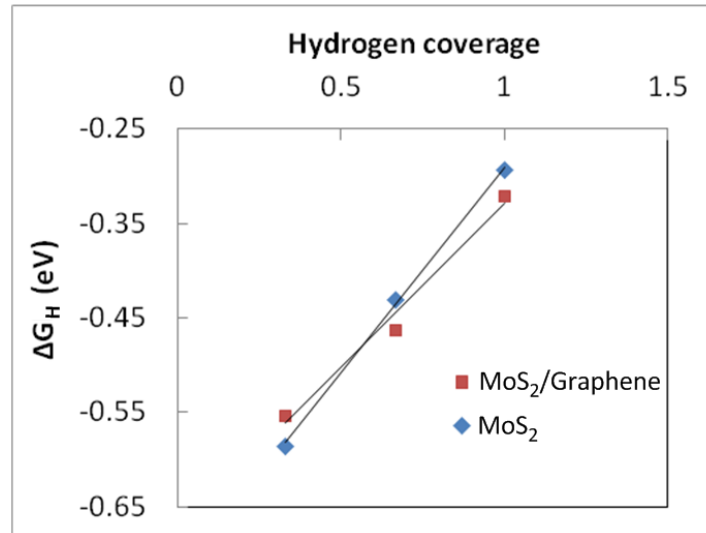


Figure 19: Hydrogen binding energy graph. Hydrogen binding energy changes as a function of hydrogen coverage.

At low coverages (< 0.5 ML), MoS₂/Graphene showed a stronger hydrogen binding than MoS₂, while at higher coverages (>0.5 ML), MoS₂/Graphene showed a weaker hydrogen binding (Figure 19). The higher the coverage, the weaker the binding. This is similar with pure metal surfaces[125]. The negative hydrogen adsorption energies for both MoS₂ and MoS₂/Graphene indicate that formation of the adsorbed hydrogen, H_{ad}, is thermodynamically downhill (the Volmer step), while the second step of HER, the formation of H₂, is the RDS. Thus, given the reaction follows the Volmer-Heyrovsky mechanism for the MoS₂ systems, the calculated hydrogen adsorption energies confirmed the experimental study of the Heyrovsky step as the RDS. Furthermore, a weaker hydrogen adsorption leads to a smaller uphill energy change for the Heyrovsky step, which makes the reaction thermodynamically more favorable. Thus on MoS₂ materials the highest coverage of hydrogen, 1 ML, is more likely in practice (Figure 20).

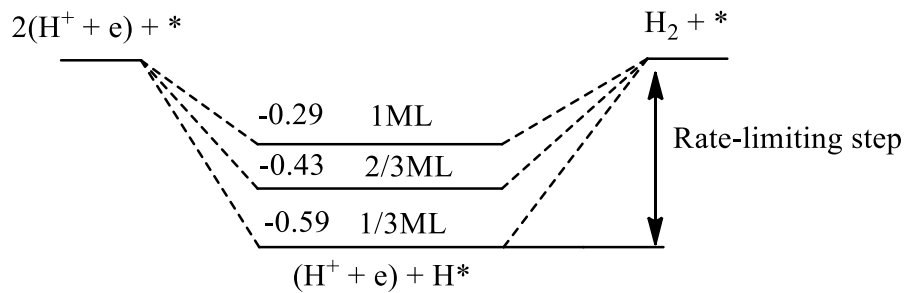


Figure 20: Reaction free energies pathway graph. Reaction free energies pathways of HER on (a) MoS₂/Graphene at different hydrogen coverages and (b) MoS₂ and MoS₂/Graphene

Also, the relationship between the theoretical MoS₂ hydrogen binding energy and the experimental HER exchange current density is studied in this work (Figure 21). Previous

studies of HER on pure metal surfaces[126] have suggested that the experimental exchange current density is directly correlated with the adsorption free energy of hydrogen (Figure 21). It is notable that the measured exchange current density of the bare Mo edge of MoS₂ on graphene is higher than the previously reported MoS₂/graphene and MoS₂/Au(111), in both of which the Mo edges were sulfided. This suggests that the MoS₂ with bare Mo edge synthesized in this study has unique catalytic properties, compared to previously studied systems.

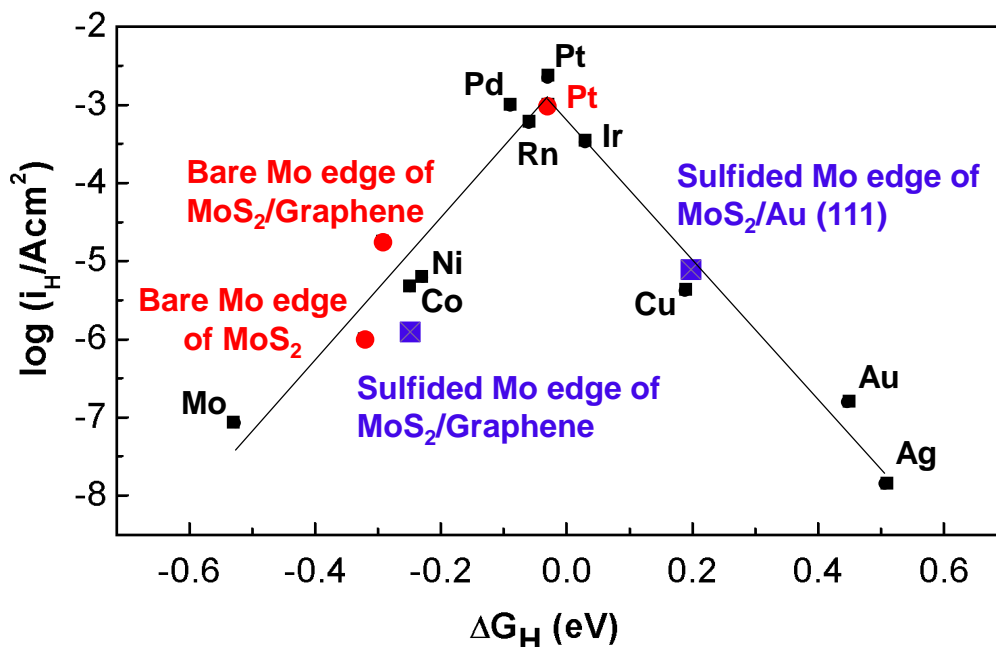


Figure 21: Activity relationship for HER. Activity relationship for the hydrogen evolution reaction (HER) showing the exchange current density as a function of the calculated free energy of hydrogen adsorption, ΔG_H . The black points are experimental data of exchange current density and computational ΔG_H [126]. The blue points represent measured rates on sulfided Mo edge of MoS₂ nanoparticles on either Au(111)[127] or graphene[128] plotted at the calculated ΔG_H [129]. The red points are the experimental data and the calculated ΔG_H from this study, in which the ΔG_H of bare Mo edge of MoS₂ (without a support) was calculated to represent the MoS₂

transferred onto glassy carbon, due to the weak interactions between MoS₂ and the support. It was assumed that surfaces with negative ΔG_H have high coverage ($\theta_H = 1$ ML) and surfaces with positive ΔG_H have low coverage ($\theta_H = 0.25$ ML), where θ_H is defined as the fraction of a monolayer with respect to the number of edge metal atoms[128], [129]. Thus in this study we use the same assumptions for the coverages.

3.3.Conclusion

The electrochemical experiments reveal a considerable enhancement on the HER activity of the MoS₂. The 3D Structured MoS₂ grown on graphene film has shown lower onset potential and higher TOF compared to 3D structured MoS₂ grown on GC and transferred to GC. DFT calculations has shown that the exchange current density of MoS₂ with bare Mo edges on graphene is higher than previously reported MoS₂ structures with sulfide edges. The observed improvement is mainly attributed to the high number of active edge sites of 3D structured MoS₂, enhanced charge transfer toward active edge atoms and optimized hydrogen binding energy due to the presence of graphene.

Chapter 4: Conclusion and future work

In conclusion, a large-area crystalline 3D structured MoS₂ is directly grown on top of the graphene film by an APCVD technique. The STEM and SEM characterizations illustrate that 3D structured MoS₂ is a layered material. These characterizations confirm the epitaxial growth of this structure on top of the graphene film. Performing control experiments and Raman study reveal that this structure grows based on the Stranski-Krastanov mode. The growth of 3D structured MoS₂ results in considerably increasing the active edge atoms compared to single-layer and bulk MoS₂. Furthermore, SEM results have shown that more compact 3D structured MoS₂ is grown on top of the graphene flakes than bare substrate. This results in having more MoS₂ active edge sites on the graphene film with the same geometrical area. The CV experiments show an onset potential of 70mv, which is very close to the onset potential of the platinum, the best known catalyst for HER. The study of the Tafel slope, for the grown structure, has shown that the Volmer-Heyrovsky is a dominant mechanism of the reaction and Heyrovsky step is the rate determining step. Furthermore, electrochemical impedance spectroscopy studies illustrate that the charge transfer resistance for MoS₂ grown on graphene film was much lower than MoS₂ directly grown on glassy carbon and transferred to glassy carbon. Also, the turn over frequency of the 3D structured MoS₂ grown on graphene is much higher than the other two tested catalysts. The stability test exhibits only 5% current density decay at overpotential of 15 mv proving the high stability of the grown structure. The DFT calculation has shown that the exchange current density for Mo terminated

edge 3D structured MoS_2 grown on top of graphene film is higher than previously reported MoS_2/Gr and MoS_2/Au (111) structures with sulfided Mo edges. The observed improvements is mainly attributed to a high number of active edge sites of 3D structured MoS_2 , enhanced charge transfer toward active edge atoms and optimized hydrogen binding energy due to the presence of graphene. The ability to directly grow these 3D structures over a wide range of substrates enables ready assimilation of these new materials in any arbitrary platform for various energy conversion and storage technologies.

For future studies, we are intended to continue this work in two separate phases: (i) testing 3D Structured MoS_2/Gr heterostructure for other electrochemical applications such as oxidation and CO_2 reduction reactions; (ii) synthesizing 3D structures of the other 2D materials like WS_2 , which has higher electronegativity of the edge atoms (W) and lower work function compared with MoS_2 , making their heterostructures with graphene and testing them for different electrochemical applications.

Cited literature

- [1] A. Behranginia, M. Asadi, C. Liu, P. Yasaei, B. Kumar, P. Phillips, T. Foroozan, J. C. Waranius, K. Kim, J. Abiade, R. F. Klie, L. A. Curtiss, and A. Salehi-Khojin, “Highly Efficient Hydrogen Evolution Reaction Using Crystalline Layered Three Dimensional Molybdenum Disulfides Grown On Graphene Film,” *Chem. Mater.*, p. acs.chemmater.5b03997, 2015.
- [2] M. G. Walter, E. L. Warren, J. R. McKone, S. W. Boettcher, Q. Mi, E. A. Santori, and N. S. Lewis, “Solar Water Splitting Cells,” *Chem. Rev. (Washington, DC, United States)*, vol. 110, no. 11, pp. 6446–6473, 2010.
- [3] A. J. Bard and M. A. Fox, “Artificial Photosynthesis: Solar Splitting of Water to Hydrogen and Oxygen Water Splitting,” *Acc. Chem. Res*, vol. 28, pp. 141–145, 1995.
- [4] J. Yang and H. S. Shin, “Recent advances in layered transition metal dichalcogenides for hydrogen evolution reaction,” *J. Mater. Chem. A*, vol. 2, no. 17, pp. 5979–5985, 2014.
- [5] Y. Yan, B. Xia, Z. Xu, and X. Wang, “Recent development of molybdenum sulfides as advanced electrocatalysts for hydrogen evolution reaction,” *ACS Catal.*, vol. 4, no. 6, pp. 1693–1705, 2014.
- [6] D. Merki and X. Hu, “Recent developments of molybdenum and tungsten sulfides as hydrogen evolution catalysts,” *Energy Environ. Sci.*, vol. 4, no. 10, p. 3878,

2011.

- [7] A. B. Laursen, S. Kegnaes, S. Dahl, and I. Chorkendorff, “Molybdenum sulfides—efficient and viable materials for electro - and photoelectrocatalytic hydrogen evolution,” *Energy Environ. Sci.*, vol. 5, no. 2, p. 5577, 2012.
- [8] M. Chhowalla, H. S. Shin, G. Eda, L.-J. Li, K. P. Loh, and H. Zhang, “The chemistry of two-dimensional layered transition metal dichalcogenide nanosheets,” *Nat. Chem.*, vol. 5, no. 4, pp. 263–275, 2013.
- [9] M. J. Allen, V. C. Tung, and R. B. Kaner, “Honeycomb carbon: A review of graphene,” *Chem. Rev.*, vol. 110, no. 1, pp. 132–145, 2010.
- [10] K. S. Novoselov, A. K. Geim, S. V Morozov, D. Jiang, Y. Zhang, S. V Dubonos, I. V Grigorieva, A. A. Firsov, a. a. F. K.S. Novoselov¹, A.K. Geim¹, S.V. Morozov², D. Jiang¹, Y. Zhang¹, S.V. Dubonos², I.V.Grigorieva¹, and K. Using, “Electric Field Effect in Atomically Thin Carbon Films,” *Science (80-.)*, vol. 306, no. 5696, pp. 666–669, 2004.
- [11] K. S. Novoselov, V. I. Fal’ko, L. Colombo, P. R. Gellert, M. G. Schwab, and K. Kim, “A roadmap for graphene,” *Nature*, vol. 490, no. 7419, pp. 192–200, 2012.
- [12] A. S. Mayorov, R. V. Gorbachev, S. V. Morozov, L. Britnell, R. Jalil, L. a. Ponomarenko, P. Blake, K. S. Novoselov, K. Watanabe, T. Taniguchi, and a. K. Geim, “Micrometer-scale ballistic transport in encapsulated graphene at room temperature,” *Nano Lett.*, vol. 11, no. 6, pp. 2396–2399, 2011.

- [13] A. a Balandin, S. Ghosh, W. Bao, I. Calizo, D. Teweldebrhan, F. Miao, and C. N. Lau, "Superior Thermal Conductivity of Single-Layer Graphene 2008," *Nano Lett.*, vol. 8, pp. 902–907, 2008.
- [14] C. Lee, X. Wei, J. W. Kysar, and J. Hone, "of Monolayer Graphene," vol. 321, no. July, pp. 385–388, 2008.
- [15] F. Bonaccorso, Z. Sun, T. Hasan, and A. C. Ferrari, "Graphene Photonics and Optoelectronics," *Nat. Photonics*, vol. 4, no. 9, pp. 611–622, 2010.
- [16] O. V. Yazyev and Y. P. Chen, "Polycrystalline graphene and other two-dimensional materials," *Nat. Nanotechnol.*, vol. 9, no. 10, pp. 755–767, 2014.
- [17] F. Schwierz, "Graphene transistors," *Nat. Nanotechnol.*, vol. 5, no. 7, pp. 487–496, 2010.
- [18] D. R. Dreyer, R. S. Ruoff, and C. W. Bielawski, "From conception to realization: An historial account of graphene and some perspectives for its future," *Angew. Chemie - Int. Ed.*, vol. 49, no. 49, pp. 9336–9344, 2010.
- [19] W. Gao, "The chemistry of graphene oxide," *Graphene Oxide Reduct. Recipes, Spectrosc. Appl.*, pp. 61–95, 2015.
- [20] S. Stankovich, D. A. Dikin, R. D. Piner, K. A. Kohlhaas, A. Kleinhammes, Y. Jia, Y. Wu, S. T. Nguyen, and R. S. Ruoff, "Synthesis of graphene-based nanosheets via chemical reduction of exfoliated graphite oxide," *Carbon N. Y.*, vol. 45, no. 7, pp. 1558–1565, 2007.

- [21] S. Park, R. S. Ruoff, and M. Engineering, "Chemical methods for the production of graphenes.," *Nat. Nanotechnol.*, vol. 4, no. 4, pp. 217–224, 2009.
- [22] I. Forbeaux, J.-M. Themlin, and J.-M. Debever, "Heteroepitaxial graphite on 6H-SiC(0001): Interface formation through conduction-band electronic structure," *Phys. Rev. B*, vol. 58, no. 24, pp. 16396–16406, 1998.
- [23] C. Berger, Z. Song, T. Li, X. Li, A. Y. Ogbazghi, R. Feng, Z. Dai, A. N. Marchenkov, E. H. Conrad, P. N. First, and W. a de Heer, "Ultrathin Epitaxial Graphite: 2D Electron Gas Properties and a Route toward Graphene-based Nanoelectronics," *J. Phys. Chem. B*, vol. 108, no. 52, pp. 19912–19916, 2004.
- [24] T. Ohta, A. Bostwick, T. Seyller, K. Horn, and E. Rotenberg, "Controlling the electronic structure of bilayer graphene.," *Science*, vol. 313, no. 5789, pp. 951–954, 2006.
- [25] C. Virojanadara, M. Syväjärvi, R. Yakimova, L. I. Johansson, A. A. Zakharov, and T. Balasubramanian, "Homogeneous large-area graphene layer growth on $6\text{H-SiC}(0001)$," *Phys. Rev. B*, vol. 78, no. 24, p. 245403, 2008.
- [26] X. Li, W. Cai, J. An, S. Kim, J. Nah, D. Yang, R. Piner, A. Velamakanni, I. Jung, E. Tutuc, S. K. Banerjee, L. Colombo, and R. S. Ruoff, "Large-area synthesis of high-quality and uniform graphene films on copper foils.," *Science (80-.)*, vol. 324, no. 5932, pp. 1312–1314, 2009.

- [27] I. Vlassiouk, M. Regmi, P. Fulvio, S. Dai, P. Datskos, G. Eres, and S. Smirnov, “Role of Hydrogen in Chemical Vapor Deposition Growth of Large Single-Crystal Graphene,” *ACS Nano*, vol. 5, no. 7, pp. 6069–6076, 2011.
- [28] I. Vlassiouk, S. Smirnov, M. Regmi, S. P. Surwade, N. Srivastava, R. Feenstra, G. Eres, C. Parish, N. Lavrik, P. Datskos, S. Dai, and P. Fulvio, “Graphene nucleation density on copper: Fundamental role of background pressure,” *J. Phys. Chem. C*, vol. 117, no. 37, pp. 18919–18926, 2013.
- [29] M. Massicotte, V. Yu, E. Whiteway, D. Vatnik, and M. Hilke, “Quantum Hall effect in fractal graphene: growth and properties of graphlocons,” *Nanotechnology*, vol. 24, no. 32, p. 325601, 2013.
- [30] B. Wu, D. Geng, Z. Xu, Y. Guo, L. Huang, Y. Xue, J. Chen, G. Yu, and Y. Liu, “Self-organized graphene crystal patterns,” *NPG Asia Mater.*, vol. 5, no. 2, p. e36, 2013.
- [31] J. Tian, H. Cao, W. Wu, Q. Yu, and Y. P. Chen, “Direct imaging of graphene edges: Atomic structure and electronic scattering,” *Nano Lett.*, vol. 11, no. 9, pp. 3663–3668, 2011.
- [32] Q. Yu, L. A. Jauregui, W. Wu, R. Colby, J. Tian, Z. Su, H. Cao, Z. Liu, D. Pandey, D. Wei, T. F. Chung, P. Peng, N. P. Guisinger, E. A. Stach, J. Bao, S.-S. Pei, and Y. P. Chen, “Control and characterization of individual grains and grain boundaries in graphene grown by chemical vapour deposition,” *Nat. Mater.*, vol.

- 10, no. 6, pp. 443–449, 2011.
- [33] A. K. Geim, “Graphene : Status and Prospects,” vol. 1530, no. 2009, pp. 1530–1534, 2010.
- [34] C. Koch, I. Ovid’ko, S. Seal, and S. Veprek, *Structural Nanocrystalline Materials*. Cambridge University Press, 2007.
- [35] J. P. Hirth and J. Lothe, *Theory of dislocations [by] John Price Hirth [and] Jens Lothe*. New York: McGraw-Hill, 1967.
- [36] I. Ovid’ko, “Mechanical Properties of Graphene,” *Rev. Adv. Mater. Sci.*, vol. 34, pp. 1–11, 2013.
- [37] P. Y. Huang, C. S. Ruiz-Vargas, A. M. van der Zande, W. S. Whitney, M. P. Levendorf, J. W. Kevek, S. Garg, J. S. Alden, C. J. Hustedt, Y. Zhu, J. Park, P. L. McEuen, and D. A. Muller, “Grains and grain boundaries in single-layer graphene atomic patchwork quilts,” *Nature*, vol. 469, no. 7330, pp. 389–392, 2011.
- [38] C. S. Ruiz-Vargas, H. L. Zhuang, P. Y. Huang, A. M. van der Zande, S. Garg, P. L. McEuen, D. a Muller, R. G. Hennig, and J. Park, “Softened elastic response and unzipping in chemical vapor deposition graphene membranes.,” *Nano Lett.*, vol. 11, no. 6, pp. 2259–63, 2011.
- [39] G. Lee, R. C. Cooper, S. J. An, S. Lee, A. Van Der Zande, N. Petrone, A. G. Hammerberg, C. Lee, B. Crawford, W. Oliver, J. W. Kysar, and J. Hone, “REPORTS High-Strength Chemical-Vapor – Deposited Graphene and Grain

- Boundaries,” vol. 340, no. May, pp. 1073–1077, 2013.
- [40] P. May, U. Khan, A. O’Neill, and J. N. Coleman, “Approaching the theoretical limit for reinforcing polymers with graphene,” *J. Mater. Chem.*, vol. 22, no. 4, p. 1278, 2012.
- [41] X. Zhao, Q. Zhang, D. Chen, and P. Lu, “Enhanced Mechanical Properties of Graphene-Based Poly(vinyl alcohol) Composites,” *Macromolecules*, vol. 43, no. 5, pp. 2357–2363, 2010.
- [42] M. A. Rafiee, J. Rafiee, I. Srivastava, Z. Wang, H. Song, Z. Z. Yu, and N. Koratkar, “Fracture and Fatigue in Graphene Nanocomposites,” *Small*, vol. 6, no. 2, pp. 179–83, 2010.
- [43] J. Liang, Y. Huang, L. Zhang, Y. Wang, Y. Ma, T. Guo, and Y. Chen, “Molecular-Level Dispersion of Graphene into Poly(vinyl alcohol) and Effective Reinforcement of their Nanocomposites,” *Adv. Funct. Mater.*, vol. 19, no. 14, pp. 2297–2302, 2009.
- [44] T. Kuilla, S. Bhadra, D. H. Yao, N. H. Kim, S. Bose, and J. H. Lee, “Recent advances in graphene based polymer composites,” *Prog. Polym. Sci.*, vol. 35, no. 11, pp. 1350–1375, 2010.
- [45] L. S. Walker, V. R. Marotto, M. A. Rafiee, N. Koratkar, and E. L. Corral, “Toughening in graphene ceramic composites,” *ACS Nano*, vol. 5, no. 4, pp. 3182–3190, 2011.

- [46] j bthundx, “Moore’s Paper,” *Electronics*, vol. 38, no. 8, 1965.
- [47] F. Schwierz, H. Wong, and J. J. Liou, *Nanometer CMOS*. Singapore: Pan Stanford Publishing, 2010.
- [48] Y. Taur and T. H. Ning, *Fundamentals of Modern VLSI Devices*. New York, NY, USA: Cambridge University Press, 1998.
- [49] I. Aberg and J. L. Hoyt, “Hole Transport in UTB MOSFETs in Strained-Si Directly on Insulator With Strained-Si Thickness Less Than 5 nm,” *IEEE Electron Device Lett.*, vol. 26, no. 9, pp. 661–663, 2005.
- [50] A. K. Geim and K. S. Novoselov, “The rise of graphene,” *Nat. Mater.*, pp. 183–191, 2007.
- [51] Y.-M. Lin, C. Dimitrakopoulos, K. a Jenkins, D. B. Farmer, H.-Y. Chiu, a Grill, and P. Avouris, “100-GHz transistors from wafer-scale epitaxial graphene,” *Science*, vol. 327, no. 5966, p. 662, 2010.
- [52] M. Y. Han, B. Özyilmaz, Y. Zhang, and P. Kim, “Energy band-gap engineering of graphene nanoribbons,” *Phys. Rev. Lett.*, vol. 98, no. 20, pp. 1–4, 2007.
- [53] P. Gava, M. Lazzeri, A. M. Saitta, and F. Mauri, “*Ab initio* study of gap opening and screening effects in gated bilayer graphene,” *Phys. Rev. B*, vol. 79, no. 16, p. 165431, 2009.
- [54] Z. H. Ni, T. Yu, Y. H. Lu, Y. Y. Wang, Y. P. Feng, and Z. X. Shen, “Uniaxial strain on graphene: Raman spectroscopy study and band-gap opening,” *ACS Nano*,

- vol. 2, no. 11, pp. 2301–2305, 2008.
- [55] H. Raza and E. C. Kan, “Armchair graphene nanoribbons: Electronic structure and electric-field modulation,” *Phys. Rev. B - Condens. Matter Mater. Phys.*, vol. 77, no. 24, pp. 1–5, 2008.
- [56] M. N. McCain, B. He, J. Sanati, Q. Jane Wang, and T. J. Marks, “Aerosol-assisted chemical vapor deposition of lubricating MoS₂ films. Ferrous substrates and titanium film doping,” *Chem. Mater.*, vol. 20, no. 16, pp. 5438–5443, 2008.
- [57] M. M. Thackeray, J. O. Thomas, and M. S. Whittingham, “Science and Applications of Mixed Conductors for Lithium Batteries,” *MRS Bull.*, vol. 25, no. 03, pp. 39–46, Mar. 2000.
- [58] R. M. A. Lieth, Ed., *Preparation and Crystal Growth of Materials with Layered Structures*. Dordrecht: Springer Netherlands, 1977.
- [59] J. Zheng, H. Zhang, S. Dong, Y. Liu, C. Tai Nai, H. Suk Shin, H. Young Jeong, B. Liu, and K. Ping Loh, “High yield exfoliation of two-dimensional chalcogenides using sodium naphthalenide,” *Nat. Commun.*, vol. 5, pp. 1–7, 2014.
- [60] H. S. S. Ramakrishna Matte, A. Gomathi, A. K. Manna, D. J. Late, R. Datta, S. K. Pati, and C. N. R. Rao, “MoS₂ and WS₂ Analogues of Graphene,” *Angew. Chemie Int. Ed.*, vol. 49, no. 24, pp. 4059–4062, 2010.
- [61] Z. Zeng, Z. Yin, X. Huang, H. Li, Q. He, G. Lu, F. Boey, and H. Zhang, “Single-layer semiconducting nanosheets: high-yield preparation and device fabrication.”

Angew. Chem. Int. Ed. Engl., vol. 50, no. 47, pp. 11093–7, Nov. 2011.

- [62] S. Najmaei, Z. Liu, W. Zhou, X. Zou, G. Shi, S. Lei, B. I. Yakobson, J. Idrobo, P. M. Ajayan, and J. Lou, “Vapour phase growth and grain boundary structure of molybdenum disulphide atomic layers.,” *Nat. Mater.*, vol. 12, pp. 754–9, 2013.
- [63] A. M. van der Zande, P. Y. Huang, D. a Chenet, T. C. Berkelbach, Y. You, G.-H. Lee, T. F. Heinz, D. R. Reichman, D. a Muller, and J. C. Hone, “Grains and grain boundaries in highly crystalline monolayer molybdenum disulphide.,” *Nat. Mater.*, vol. 12, no. 6, pp. 554–61, Jun. 2013.
- [64] J. D. Benck, T. R. Hellstern, J. Kibsgaard, P. Chakthranont, and T. F. Jaramillo, “Catalyzing the Hydrogen Evolution Reaction (HER) with Molybdenum Sulfi de Nanomaterials,” *ACS Catal.*, vol. 4, no. 11, pp. 3957–3971, 2014.
- [65] K. Mak, C. Lee, J. Hone, J. Shan, and T. Heinz, “Atomically Thin MoS₂: A New Direct-Gap Semiconductor,” *Physical Review Letters*, vol. 105, no. 13. p. 136805, Sep-2010.
- [66] A. Splendiani, L. Sun, Y. Zhang, T. Li, J. Kim, C.-Y. Chim, G. Galli, and F. Wang, “Emerging photoluminescence in monolayer MoS₂.,” *Nano Lett.*, vol. 10, no. 4, pp. 1271–5, Apr. 2010.
- [67] B. Radisavljevic, a Radenovic, J. Brivio, V. Giacometti, and a Kis, “Single-layer MoS₂ transistors.,” *Nat. Nanotechnol.*, vol. 6, no. March, pp. 147–150, 2011.
- [68] A. Allain, J. Kang, K. Banerjee, and A. Kis, “Electrical contacts to two-

- dimensional semiconductors.,” *Nat. Mater.*, vol. 14, no. 12, pp. 1195–205, 2015.
- [69] E. Kaxiras, J. Kong, and H. Wang, “Graphene/MoS₂ Hybrid Technology for Large-Scale Two- Dimensional Electronics,” *Nano Lett.*, vol. 14, no. Cvd, pp. 3055–3063, 2014.
- [70] Y. Liu, H. Wu, H.-C. Cheng, S. Yang, E. Zhu, Q. He, M. Ding, D. Li, J. Guo, N. O. Weiss, Y. Huang, and X. Duan, “Toward Barrier Free Contact to Molybdenum Disulfide Using Graphene Electrodes,” *Nano Lett.*, vol. 15, no. 5, pp. 3030–3034, 2015.
- [71] R. Kappera, D. Voiry, S. E. Yalcin, B. Branch, G. Gupta, A. D. Mohite, and M. Chhowalla, “Phase-engineered low-resistance contacts for ultrathin MoS₂ transistors,” *Nat. Mater.*, vol. 13, no. 12, pp. 1128–1134, 2014.
- [72] K. S. Novoselov, D. Jiang, F. Schedin, T. J. Booth, V. V Khotkevich, S. V Morozov, and a K. Geim, “Two-dimensional atomic crystals.,” *Proc. Natl. Acad. Sci. U. S. A.*, vol. 102, no. 30, pp. 10451–10453, 2005.
- [73] I. Song, C. Park, and H. C. Choi, “Synthesis and properties of molybdenum disulphide: from bulk to atomic layers,” *RSC Adv.*, vol. 5, no. 10, pp. 7495–7514, 2015.
- [74] R. J. Smith, P. J. King, M. Lotya, C. Wirtz, U. Khan, S. De, A. O’Neill, G. S. Duesberg, J. C. Grunlan, G. Moriarty, J. Chen, J. Wang, A. I. Minett, V. Nicolosi, and J. N. Coleman, “Large-scale exfoliation of inorganic layered compounds in

- aqueous surfactant solutions,” *Adv. Mater.*, vol. 23, no. 34, pp. 3944–3948, 2011.
- [75] P. Afanasiev, G.-F. Xia, G. Berhault, B. Jouguet, and M. Lacroix, “Surfactant-Assisted Synthesis of Highly Dispersed Molybdenum Sulfide,” *Chem. Mater.*, vol. 11, no. 11, pp. 3216–3219, 1999.
- [76] N. Liu, P. Kim, J. H. Kim, J. H. Ye, S. Kim, and C. J. Lee, “Large-area atomically thin MoS₂ nanosheets prepared using electrochemical exfoliation,” *ACS Nano*, vol. 8, no. 7, pp. 6902–6910, 2014.
- [77] K. K. Liu, W. Zhang, Y. H. Lee, Y. C. Lin, M. T. Chang, C. Y. Su, C. S. Chang, H. Li, Y. Shi, H. Zhang, C. S. Lai, and L. J. Li, “Growth of large-area and highly crystalline MoS₂ thin layers on insulating substrates,” *Nano Lett.*, vol. 12, pp. 1538–1544, 2012.
- [78] Y. Zhan, Z. Liu, S. Najmaei, P. M. Ajayan, and J. Lou, “Large-area vapor-phase growth and characterization of MoS₂ atomic layers on a SiO₂ substrate,” *Small*, vol. 8, no. 7, pp. 966–971, 2012.
- [79] Y. H. Lee, X. Q. Zhang, W. Zhang, M. T. Chang, C. Te Lin, K. Di Chang, Y. C. Yu, J. T. W. Wang, C. S. Chang, L. J. Li, and T. W. Lin, “Synthesis of large-area MoS₂ atomic layers with chemical vapor deposition,” *Adv. Mater.*, vol. 24, no. 17, pp. 2320–2325, May 2012.
- [80] A. H. Castro Neto, “Charge density wave, superconductivity, and anomalous metallic behavior in 2D transition metal dichalcogenides,” *Phys. Rev. Lett.*, vol.

86, no. 19, pp. 4382–4385, 2001.

- [81] S. Balendhran, J. Z. Ou, M. Bhaskaran, S. Sriram, S. Ippolito, Z. Vasic, E. Kats, S. Bhargava, S. Zhuiykov, and K. Kalantar-Zadeh, “Atomically thin layers of MoS₂ via a two step thermal evaporation-exfoliation method,” *Nanoscale*, vol. 4, no. 2, pp. 461–466, 2012.
- [82] Y. Shi, W. Zhou, A.-Y. Lu, W. Fang, Y.-H. Lee, A. L. Hsu, S. M. Kim, K. K. Kim, H. Y. Yang, L.-J. Li, J.-C. Idrobo, and J. Kong, “van der Waals Epitaxy of MoS₂ Layers Using Graphene as Growth Templates,” *Nano Lett.*, vol. 12, pp. 2784–2791, 2012.
- [83] Q. H. Wang, K. Kalantar-Zadeh, A. Kis, J. N. Coleman, and M. S. Strano, “Electronics and optoelectronics of two-dimensional transition metal dichalcogenides,” *Nat. Nanotechnol.*, vol. 7, no. 11, pp. 699–712, 2012.
- [84] S. Bertolazzi, J. Brivio, and A. Kis, “Stretching and breaking of ultrathin MoS₂,” *ACS Nano*, vol. 5, no. 12, pp. 9703–9709, 2011.
- [85] H. S. Lee, S. W. Min, Y. G. Chang, M. K. Park, T. Nam, H. Kim, J. H. Kim, S. Ryu, and S. Im, “MoS₂ nanosheet phototransistors with thickness-modulated optical energy gap,” *Nano Lett.*, vol. 12, no. 7, pp. 3695–3700, 2012.
- [86] J. Greeley, T. F. Jaramillo, J. Bonde, I. B. Chorkendorff, and J. K. Nørskov, “Computational high-throughput screening of electrocatalytic materials for hydrogen evolution,” *Nat. Mater.*, vol. 5, no. 11, pp. 909–13, 2006.

- [87] J. Electroanal, “octahedron,” vol. 81, pp. 97–111.
- [88] T. F. Jaramillo, K. P. Jørgensen, J. Bonde, J. H. Nielsen, S. Horch, and I. Chorkendorff, “Identification of active edge sites for electrochemical H₂ evolution from MoS₂ nanocatalysts.,” *Science*, vol. 317, no. July, pp. 100–102, 2007.
- [89] B. Hinnemann, P. G. Moses, J. Bonde, K. P. Jorgensen, J. H. Nielsen, S. Horch, I. Chorkendorff, and J. K. Nørskov, “Biomimetic Hydrogen Evolution: {MoS}₂ Nanoparticles as Catalyst for Hydrogen Evolution,” *J. Am. Chem. Soc.*, vol. 127, no. 15, pp. 5308–5309, 2005.
- [90] Z. Chen, D. Cummins, B. N. Reinecke, E. Clark, M. K. Sunkara, and T. F. Jaramillo, “Core-shell MoO₃-MoS₂ nanowires for hydrogen evolution: A functional design for electrocatalytic materials,” *Nano Lett.*, vol. 11, no. 10, pp. 4168–4175, 2011.
- [91] D. Kong, H. Wang, J. J. Cha, M. Pasta, K. J. Koski, J. Yao, and Y. Cui, “Synthesis of MoS₂ and MoSe₂ films with vertically aligned layers,” *Nano Lett.*, vol. 13, no. 3, pp. 1341–1347, 2013.
- [92] H. S. Lee, S. W. Min, M. K. Park, Y. T. Lee, P. J. Jeon, J. H. Kim, S. Ryu, and S. Im, “MoS₂ nanosheets for top-gate nonvolatile memory transistor channel,” *Small*, vol. 8, no. 20, pp. 3111–3115, 2012.
- [93] Z. Yin, H. Li, H. Li, L. Jiang, Y. Shi, Y. Sun, G. Lu, Q. Zhang, X. Chen, and H. Zhang, “Ultrasensitive photodetectors based on monolayer MoS₂.,” *ACS Nano*,

vol. 6, no. 1, pp. 74–80, 2012.

- [94] Z. Yin, H. Li, H. Li, L. Jiang, Y. Shi, Y. Sun, G. Lu, Q. Zhang, X. Chen, and H. Zhang, “Single-layer MoS₂ phototransistors,” *ACS Nano*, vol. 6, no. 1, pp. 74–80, 2012.
- [95] D. J. Li, U. N. Maiti, J. Lim, D. S. Choi, W. J. Lee, Y. Oh, G. Y. Lee, and S. O. Kim, “Molybdenum sulfide/N-doped CNT forest hybrid catalysts for high-performance hydrogen evolution reaction,” *Nano Lett.*, vol. 14, pp. 1228–1233, 2014.
- [96] J. Kibsgaard, Z. Chen, B. N. Reinecke, and T. F. Jaramillo, “Engineering the surface structure of MoS₂ to preferentially expose active edge sites for electrocatalysis,” *Nat. Mater.*, vol. 11, no. October, pp. 963–969, 2012.
- [97] T. Stephenson, Z. Li, B. Olsen, and D. Mitlin, “Lithium ion battery applications of molybdenum disulfide (MoS₂) nanocomposites,” *Energy Environ. Sci.*, vol. 7, p. 209, 2014.
- [98] Y. H. Lee, L. Yu, H. Wang, W. Fang, X. Ling, Y. Shi, C. Te Lin, J. K. Huang, M. T. Chang, C. S. Chang, M. Dresselhaus, T. Palacios, L. J. Li, and J. Kong, “Synthesis and transfer of single-layer transition metal disulfides on diverse surfaces,” *Nano Lett.*, vol. 13, pp. 1852–1857, 2013.
- [99] A. M. van der Zande, P. Y. Huang, D. a Chenet, T. C. Berkelbach, Y. You, G.-H. Lee, T. F. Heinz, D. R. Reichman, D. a Muller, and J. C. Hone, “Grains and grain

- boundaries in highly crystalline monolayer molybdenum disulphide.,” *Nat. Mater.*, vol. 12, no. 6, pp. 554–61, Jun. 2013.
- [100] J. Xie, H. Zhang, S. Li, R. Wang, X. Sun, M. Zhou, J. Zhou, X. W. Lou, and Y. Xie, “Defect-rich MoS₂ ultrathin nanosheets with additional active edge sites for enhanced electrocatalytic hydrogen evolution,” *Adv. Mater.*, vol. 25, pp. 5807–5813, 2013.
- [101] J. Kibsgaard, T. F. Jaramillo, and F. Besenbacher, “Building an appropriate active-site motif into a hydrogen-evolution catalyst with thiomolybdate [Mo₃S₁₃]²⁻ clusters.,” *Nat. Chem.*, vol. 6, no. 3, pp. 248–53, 2014.
- [102] A. . Ferrari, J. C. Meyer, C. Scardaci, C. Casiraghi, and M. Lazzeri, “Raman Spectrum of Graphene and Graphene Layers,” *Phys. Rev. Lett.*, vol. 97, no. NOVEMBER, p. 187401 (4), 2006.
- [103] M. Asadi, B. Kumar, A. Behranginia, B. a Rosen, A. Baskin, N. Reprin, D. Pisasale, P. Phillips, W. Zhu, R. Haasch, R. F. Klie, P. Král, J. Abiade, and A. Salehi-Khojin, “Robust carbon dioxide reduction on molybdenum disulphide edges.,” *Nat. Com.*, vol. 5, p. 4470, 2014.
- [104] T. Weber, J. C. Muijsers, J. H. M. C. van Wolput, C. P. J. Verhagen, and J. W. Niemantsverdriet, “Basic Reaction Steps in the Sulfidation of Crystalline MoO₃ to MoS₂ , As Studied by X-ray Photoelectron and Infrared Emission Spectroscopy,” *J. Phys. Chem.*, vol. 100, no. 96, pp. 14144–14150, 1996.

- [105] H. Li, Q. Zhang, C. C. R. Yap, B. K. Tay, T. H. T. Edwin, A. Olivier, and D. Baillargeat, “From bulk to monolayer MoS₂: Evolution of Raman scattering,” *Adv. Funct. Mater.*, vol. 22, no. 1 L, pp. 1385–1390, 2012.
- [106] X. Wang, H. Feng, Y. Wu, and L. Jiao, “Controlled Synthesis of Highly Crystalline MoS₂ Flakes by Chemical Vapor Deposition,” *J. Am. Chem. Soc.*, vol. 135, pp. 5–8, 2013.
- [107] Y.-H. Lee, X.-Q. Zhang, W. Zhang, M.-T. Chang, C.-T. Lin, K.-D. Chang, Y.-C. Yu, J. T.-W. Wang, C.-S. Chang, L.-J. Li, and T.-W. Lin, “Synthesis of large-area MoS₂ atomic layers with chemical vapor deposition,” *Adv. Mater.*, vol. 24, no. 17, pp. 2320–5, May 2012.
- [108] B. Lewis and J. C. Anderson, *NUCLEATION AND GROWTH OF THIN FILMS*. Academic Press Inc, 1978.
- [109] J. A. Venables, *Introduction to Surface and Thin Film Processes - Cambridge University Press*. Cambridge University Press, 2000.
- [110] A. Pimpinelli and V. Jacques, *Physics of Crystal Growth*. Cambridge University Press, 1998.
- [111] K. Oura, V. G. Lifshits, A. A. Saranin, A. V Zotov, and M. Katayama, *Surface Science: An Introduction*, vol. 4, no. 7. Springer, 2003.
- [112] Y. Y. Hui, X. Liu, W. Jie, N. Y. Chan, J. Hao, Y. Te Hsu, L. J. Li, W. Guo, and S. P. Lau, “Exceptional tunability of band energy in a compressively strained trilayer

- MoS₂ sheet,” *ACS Nano*, vol. 7, no. 8, pp. 7126–7131, 2013.
- [113] Y. Yu, S.-Y. Huang, Y. Li, S. N. Steinmann, W. Yang, and L. Cao, “Layer-Dependent Electrocatalysis of MoS₂ for Hydrogen Evolution,” *Nano Lett.*, vol. 14, no. 2, pp. 553–558, Feb. 2014.
- [114] J. An, E. Voelkl, J. Suk, X. Li, C. W. Magnuson, L. Fu, P. Tiemeijer, M. Bischoff, B. Freitag, E. Popova, and R. S. Ruoff, “Domain (Grain) Boundaries and Evidence of ‘ Twin-Like ’ Structures in CVD Grown Graphene Domain (Grain) Boundaries and Evidence of ‘ Twin-Like ’ Structures in CVD Grown Graphene,” *Nano*, no. 4, pp. 2433–2439, 2011.
- [115] Y. Yang, H. Fei, G. Ruan, C. Xiang, and J. M. Tour, “Edge-Oriented MoS₂ Nanoporous Films as Flexible Electrodes for Hydrogen Evolution Reactions and Supercapacitor Devices,” *Adv. Mater.*, vol. 26, pp. 8163–8168, 2014.
- [116] D. Voiry, M. Salehi, R. Silva, T. Fujita, M. Chen, T. Asefa, V. B. Shenoy, G. Eda, and M. Chhowalla, “Conducting MoS₂ nanosheets as catalysts for hydrogen evolution reaction,” *Nano Lett.*, vol. 13, pp. 6222–7, 2013.
- [117] Y. Li, H. Wang, L. Xie, Y. Liang, G. Hong, and H. Dai, “MoS₂ nanoparticles grown on graphene: An advanced catalyst for the hydrogen evolution reaction,” *J. Am. Chem. Soc.*, vol. 133, pp. 7296–7299, 2011.
- [118] D. Gao, H. Zhou, J. Wang, S. Miao, F. Yang, G. Wang, J. Wang, and X. Bao, “Size-Dependent Electrocatalytic Reduction of CO₂ over Pd Nanoparticles,” *J.*

- Am. Chem. Soc.*, vol. 137, no. 13, pp. 4288–4291, Apr. 2015.
- [119] A. Salehi-Khojin, H. R. M. Jhong, B. a. Rosen, W. Zhu, S. Ma, P. J. a Kenis, and R. I. Masel, “Nanoparticle silver catalysts that show enhanced activity for carbon dioxide electrolysis,” *J. Phys. Chem. C*, vol. 117, no. 4, pp. 1627–1632, 2013.
- [120] H. Wang, H. S. Casalongue, Y. Liang, and H. Dai, “Ni(OH)₂ nanoplates grown on graphene as advanced electrochemical pseudocapacitor materials,” *J. Am. Chem. Soc.*, vol. 132, no. 25, pp. 7472–7477, 2010.
- [121] Y. Tan, P. Liu, L. Chen, W. Cong, Y. Ito, J. Han, X. Guo, Z. Tang, T. Fujita, A. Hirata, and M. W. Chen, “Monolayer MoS₂ Films Supported by 3D Nanoporous Metals for High-Efficiency Electrocatalytic Hydrogen Production,” *Adv. Mater.*, vol. 26, no. 47, pp. 8023–8028, 2014.
- [122] J. D. Benck, Z. Chen, L. Y. Kuritzky, A. J. Forman, and T. F. Jaramillo, “Amorphous molybdenum sulfide catalysts for electrochemical hydrogen production: Insights into the origin of their catalytic activity,” *ACS Catal.*, vol. 2, pp. 1916–1923, 2012.
- [123] G. Kresse and J. Furthmüller, “Efficiency of ab-initio total energy calculations for metals and semiconductors using a plane-wave basis set,” *Comput. Mater. Sci.*, vol. 6, no. 1, pp. 15–50, 1996.
- [124] G. Kresse, “Efficient iterative schemes for ab initio total-energy calculations using a plane-wave basis set,” *Phys. Rev. B*, vol. 54, no. 16, pp. 11169–11186, Oct.

1996.

- [125] C. Tsai, F. Abild-Pedersen, and J. K. Nørskov, “Tuning the MoS₂ edge-site activity for hydrogen evolution via support interactions,” *Nano Lett.*, vol. 14, no. 3, pp. 1381–7, Mar. 2014.
- [126] J. K. Nørskov, T. Bligaard, a. Logadottir, J. R. Kitchin, J. G. Chen, S. Pandalov, and U. Stimming, “Trends in the Exchange Current for Hydrogen Evolution,” *J. Electrochem. Soc.*, vol. 152, no. 3, p. J23, 2005.
- [127] T. F. Jaramillo, K. P. Jørgensen, J. Bonde, J. H. Nielsen, S. Hørch, and I. Chorkendorff, “Identification of active edge sites for electrochemical H₂ evolution from MoS₂ nanocatalysts,” *Science*, vol. 317, no. 5834, pp. 100–102, 2007.
- [128] J. Bonde, P. G. Moses, T. F. Jaramillo, J. K. Nørskov, and I. Chorkendorff, “Hydrogen evolution on nano-particulate transition metal sulfides,” *Faraday Discuss.*, vol. 140, pp. 219–231, Oct. 2009.
- [129] C. Tsai, F. Abild-Pedersen, and J. K. Nørskov, “Tuning the MoS₂ edge-site activity for hydrogen evolution via support interactions,” *Nano Lett.*, vol. 14, no. 3, pp. 1381–1387, 2014.

APPENDIXES

Here, the written permission from the journal of my published paper is presented. This paper has been used for the write up of this document.

For chapter 3 (reference 1):

2/1/2016 Rightslink® by Copyright Clearance Center



[Home](#) [Create Account](#) [Help](#)  [Live Chat](#)

 **ACS Publications** Most Trusted. Most Cited. Most Read.

Title: Highly Efficient Hydrogen Evolution Reaction Using Crystalline Layered Three-Dimensional Molybdenum Disulfides Grown on Graphene Film

Author: Amirhossein Behranginia, Mohammad Asadi, Cong Liu, et al

Publication: Chemistry of Materials

Publisher: American Chemical Society

Date: Jan 1, 2016

Copyright © 2016, American Chemical Society

LOGIN

If you're a copyright.com user, you can login to RightsLink using your copyright.com credentials. Already a RightsLink user or want to [learn more?](#)

PERMISSION/LICENSE IS GRANTED FOR YOUR ORDER AT NO CHARGE

This type of permission/license, instead of the standard Terms & Conditions, is sent to you because no fee is being charged for your order. Please note the following:

- Permission is granted for your request in both print and electronic formats, and translations.
- If figures and/or tables were requested, they may be adapted or used in part.
- Please print this page for your records and send a copy of it to your publisher/graduate school.
- Appropriate credit for the requested material should be given as follows: "Reprinted (adapted) with permission from (COMPLETE REFERENCE CITATION). Copyright (YEAR) American Chemical Society." Insert appropriate information in place of the capitalized words.
- One-time permission is granted only for the use specified in your request. No additional uses are granted (such as derivative works or other editions). For any other uses, please submit a new request.

[BACK](#)[CLOSE WINDOW](#)

Copyright © 2016 Copyright Clearance Center, Inc. All Rights Reserved. [Privacy statement](#). [Terms and Conditions](#). Comments? We would like to hear from you. E-mail us at customer@copyright.com

Vita

General Information:

Name: Amirhossein Behranginia

Date of Birth: 09/06/1988

Gender: Male

Education

M.Sc. Mechanical Engineering, **University of Illinois at Chicago (UIC)**, Chicago, USA

B.Sc. Mechanical Engineering, **Science and Research branch of Azad University**, Tehran, Iran

Patents and Publications

Patents:

1. A. Salehi-Khojin, **A. Behranginia**, M. Asadi, P. Yasaei, “Three-Dimensional Chemical Vapor Deposited Molybdenum Disulfide Catalyst for Hydrogen Evolution Reaction” U.S. Provisional Patent Application, Submitted

Published journal papers:

1. M. Asadi, B. Kumar, C. Liu, P. Phillips, P. Yasaei, **A. Behranginia**, P. Zapol, R. F. Klie, L. A. Curtiss, and A. Salehi-Khojin, “Cathode Based on Molybdenum Disulfide Nanoflakes for Lithium–Oxygen Batteries,” *ACS Nano*, p. acsnano.5b06672, 2016.
2. **A. Behranginia**, M. Asadi, C. Liu, P. Yasaei, B. Kumar, P. Phillips, T. Foroozan, J. C. Waranius, K. Kim, J. Abiade, R. F. Klie, L. A. Curtiss, and A. Salehi-Khojin, “Highly Efficient Hydrogen Evolution Reaction Using Crystalline Layered Three Dimensional Molybdenum Disulfides Grown On Graphene Film,” *Chem. Mater.*, p. acs.chemmater.5b03997, 2015.
3. P. Yasaei, **A. Behranginia**, T. Foroozan, M. Asadi, K. Kim, F. Khalili-Araghi, and A. Salehi-Khojin, “Stable and Selective Humidity Sensing Using Stacked Black Phosphorus Flakes,” *ACS Nano*, vol. 9, no. 10, pp. 9898–9905, 2015.
4. M. Asadi, B. Kumar, **A. Behranginia**, B. a Rosen, A. Baskin, N. Repnin, D. Pisasale, P. Phillips, W. Zhu, R. Haasch, R. F. Klie, P. Král, J. Abiade, and A. Salehi-Khojin, “Robust carbon dioxide reduction on molybdenum disulphide edges,” *Nat. Com.*, vol. 5, p. 4470, 2014.

5. M. Purahmad, J. Huang, M. Plakhotnyuk, X. Zhang, J. Lee, **A. Behranginia**, P. Yasaei, T. Durowade, K. Spratt, M. Silvestri, M. Gouk, X. Cui, S. Chang, K. Maamari, M. Mathur, A. Solat, H. Tahiru, N. Krzyzanowski, A. Meyer, J. Counts, E. Tsang, N. Strach, I. Mohedano, M. Valencia, A. Raghunathan, T. Dankovic, A. Feinerman, and H. Busta, "A MEMS-based resistive vacuum gauge with voltage readout," *2013 26th Int. Vac. Nanoelectron. Conf. IVNC 2013*, pp. 3–4, 2013.

Submitted manuscripts:

A. Behranginia, P. Yasaei, A.K. Majee, F. Long, C.J. Foss, T. Foroozan, S. Fuladi, M. Hantehzadeh, R. Shahbazian-Yassar, Z. Aksamija, A. Salehi-Khojin, "Direct-Grown Graphene and Molybdenum Disulfide Lateral Heterostructures for Highly-Packed All-Two Dimensional Electronic Circuitry," *Nat. Nanotechnol.*, Submitted, 2016.

Conference Proceedings:

Amirhossein Behranginia, Mohammad Asadi, Amin Salehi-Khojin, "Three Dimensional Molybdenum Disulfides Grown on Monolayer Graphene for Hydrogen Evolution Reaction" Material Research Society (MRS), Boston, MA, Fall 2015.

Technical Experience

Jan. 2013- Present	Research assistant , " <i>Nanomaterials and Energy Systems Lab</i> " UIC
Aug. 2014- Dec. 2014	Teaching assistant & lab instructor , " <i>Introduction to Heat Transfer</i> ", UIC
Jan. 2014- May. 2014	Teaching assistant , " <i>Intermediate thermodynamics</i> ", UIC
Jan. 2013- May. 2013	Teaching assistant , " <i>Introduction to thermodynamics</i> ", UIC

Professional Membership

-
- American Society of Mechanical Engineers (ASME)
 - American Institute of Chemical Engineers (AIChE)
 - Materials Research Society (MRS)